






## ARTICLE



## gp120-derived amyloidogenic peptides form amyloid fibrils that increase HIV-1 infectivity

Suiyi Tan<sup>1,10</sup>, Wenjuan Li<sup>1,10</sup>, Chan Yang<sup>1,10</sup>, Qingping Zhan<sup>1</sup>, Kunyu Lu<sup>1</sup>, Jun Liu<sup>2</sup>, Yong-Mei Jin<sup>2</sup>, Jin-Song Bai<sup>2</sup>, Lin Wang<sup>3</sup>, Jinqing Li<sup>1</sup>, Zhaofeng Li<sup>1</sup>, Fei Yu<sup>4</sup>, Yu-Ye Li<sup>5</sup>, Yue-Xun Duan<sup>6</sup>, Lu Lu<sup>7</sup>, Tong Zhang<sup>8</sup>, Jiaqi Wei<sup>8</sup>, Lin Li<sup>1</sup>, Yong-Tang Zheng<sup>9</sup>, Shibo Jiang<sup>7</sup> and Shuwen Liu<sup>1</sup>

© The Author(s), under exclusive licence to CSI and USTC 2024

Apart from mediating viral entry, the function of the free HIV-1 envelope protein (gp120) has yet to be elucidated. Our group previously showed that EP2 derived from one  $\beta$ -strand in gp120 can form amyloid fibrils that increase HIV-1 infectivity. Importantly, gp120 contains ~30  $\beta$ -strands. We examined whether gp120 might serve as a precursor protein for the proteolytic release of amyloidogenic fragments that form amyloid fibrils, thereby promoting viral infection. Peptide array scanning, enzyme degradation assays, and viral infection experiments in vitro confirmed that many  $\beta$ -stranded peptides derived from gp120 can indeed form amyloid fibrils that increase HIV-1 infectivity. These gp120-derived amyloidogenic peptides, or GAPs, which were confirmed to form amyloid fibrils, were termed gp120-derived enhancers of viral infection (GEVIs). GEVIs specifically capture HIV-1 virions and promote their attachment to target cells, thereby increasing HIV-1 infectivity. Different GAPs can cross-interact to form heterogeneous fibrils that retain the ability to increase HIV-1 infectivity. GEVIs even suppressed the antiviral activity of a panel of antiretroviral agents. Notably, endogenous GAPs and GEVIs were found in the lymphatic fluid, lymph nodes, and cerebrospinal fluid (CSF) of AIDS patients in vivo. Overall, gp120-derived amyloid fibrils might play a crucial role in the process of HIV-1 infectivity and thus represent novel targets for anti-HIV therapeutics.

**Keywords:** HIV-1; gp120; Amyloid fibril; Enhancement of viral infectivity

*Cellular & Molecular Immunology* (2024) 21:479–494; <https://doi.org/10.1038/s41423-024-01144-y>

## INTRODUCTION

The spike protein of HIV-1 consists of three gp120 envelope glycoproteins noncovalently attached to three gp41 transmembrane glycoproteins on the surface of virions or infected cells. Gp120 is essential for viral entry because it binds to the receptor CD4 and a coreceptor (CCR5 or CXCR4) on target cells to trigger subsequent membrane fusion [1]. Free gp120 is also reported to induce inflammation [2], apoptosis [3], and pyroptosis [4] in various cell lines. Therefore, gp120 is associated with various pathogenic consequences in vivo, including neurodegenerative disorders [5], endothelial dysfunction [6], barrier disruption [7], and bone abnormalities [8]. Several reports have suggested that gp120 shedding plays an important role in the pathogenesis of HIV-1.

Amyloids are highly ordered  $\beta$ -sheet-rich protein/peptide assemblies deposited in different organs and tissues. These assemblies have been linked to a variety of human diseases, including

neurodegenerative disorders and systemic and local diseases [9]. They are also highly linked to infectious disease. Some are themselves infectious, such as prions and amyloid- $\beta$  (A $\beta$ ), tau, and  $\alpha$ -Syn, which show prion-like spread [10, 11]. Some are enhancers of microbial infections, including bacteria, fungi, and viruses [12–14]. Seminal proteins, such as prostatic acidic phosphatase and semenogelins, are proteolyzed in vivo to release amyloidogenic fragments that form amyloid fibrils, which, in turn, exhibit a cationic surface that could intensify HIV-1 infectivity [14, 15]. Several chemicals targeting these seminal amyloid fibrils have been reported [16]. We also found that peptides derived from the gp120 coreceptor binding domain can form amyloid fibrils that promote HIV-1 infection. These peptides are named enhancing peptides (EPs) [17].

The extended cross- $\beta$  amyloid motif constitutes the basic structure of amyloid fibrils [18]. As previously noted, the HIV-1 gp120 subunit consists of 30  $\beta$ -strands [19, 20]. These  $\beta$ -strands

<sup>1</sup>Guangdong-Hong Kong-Macao Joint Laboratory for New Drug Screening, NMPA Key Laboratory for Research and Evaluation of Drug Metabolism, Guangdong Provincial Key Laboratory of New Drug Screening, School of Pharmaceutical Sciences, Southern Medical University, Guangzhou 510515, China. <sup>2</sup>Department of Infectious Disease, The Third People's Hospital of Kunming, Kunming 650041, China. <sup>3</sup>Department of Pathology, The Third People's Hospital of Kunming, Kunming 650041, China. <sup>4</sup>Hebei Key Laboratory of Analysis and Control of Zoonotic Pathogenic Microorganism, College of Life Sciences, Hebei Agricultural University, Baoding 071001, China. <sup>5</sup>Department of Dermatology and Venereology, First Affiliated Hospital of Kunming Medical University, Kunming 650032, China. <sup>6</sup>Yunnan Provincial Infectious Disease Hospital, Kunming 650301, China. <sup>7</sup>Key Laboratory of Medical Molecular Virology (MOE/NHC/CAMS), Shanghai Institute of Infectious Disease and Biosecurity, School of Basic Medical Sciences, Fudan University, Shanghai 200032, China. <sup>8</sup>Beijing Key Laboratory for HIV/AIDS Research, Clinical and Research Center for Infectious Diseases, Beijing Youan Hospital, Capital Medical University, Beijing 100069, China. <sup>9</sup>State Key Laboratory of Genetic Evolution & Animal Models, Key Laboratory of Bioactive Peptides of Yunnan Province, KIZ-CUHK Joint Laboratory of Bioresources and Molecular Research in Common Diseases, Center for Biosafety Mega-Science, Kunming Institute of Zoology, Chinese Academy of Sciences, Kunming, Yunnan 650223, China. <sup>10</sup>These authors contributed equally: Suiyi Tan, Wenjuan Li, Chan Yang. ✉email: [suiyitan@smu.edu.cn](mailto:suiyitan@smu.edu.cn); [shibojiang@fudan.edu.cn](mailto:shibojiang@fudan.edu.cn); [liusw@smu.edu.cn](mailto:liusw@smu.edu.cn)

Received: 13 July 2023 Accepted: 2 February 2024

Published online: 5 March 2024

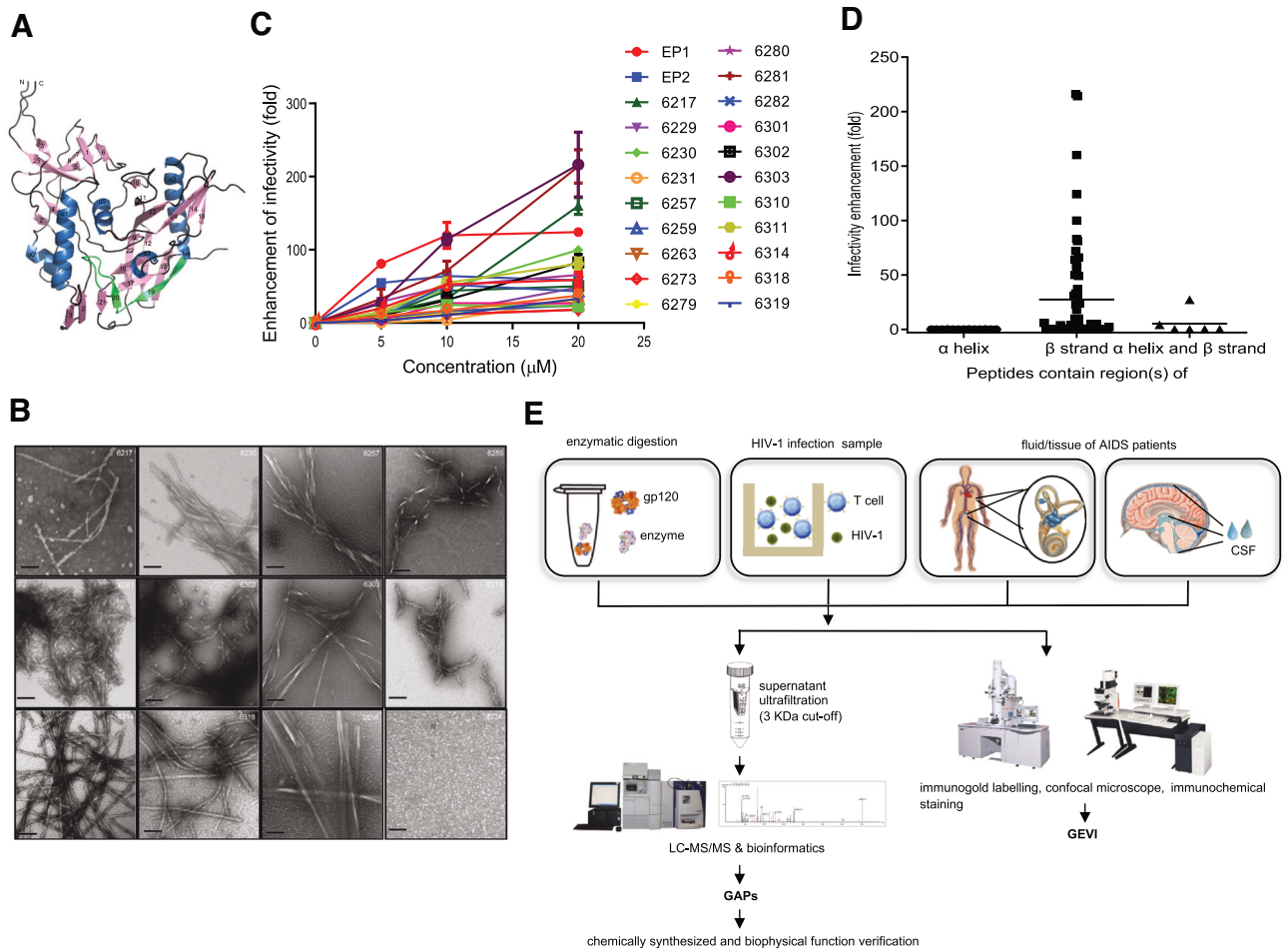


**Fig. 1** Peptides derived from  $\beta$ -strands in HIV-1 gp120 form amyloid fibrils that strongly increase HIV-1 infectivity. **A** Ribbon diagram of gp120.  $\beta$ -Strands of the core gp120 are shown as arrows and are depicted in pink. The  $\alpha$ -helices are depicted in blue.  $\beta$ 1;  $\beta$ 4;  $\beta$ 0 and  $\beta$ 15 are not displayed. Strands  $\beta$ 19 and  $\beta$ 20, which overlap the sequences of peptides EP1, EP2 and EP3, are highlighted in green. **B** Electron micrographs of amyloid fibrils formed by fragments of  $\beta$ -strands in HIV-1 MN gp120. The numbers at the top right of the pictures correspond to the peptide number of the HIV-1 MN envelope peptide set. Images are shown relative to a scale bar of 100 nm. SEVIs (PAP248-286) and peptide 6324 from the  $\alpha$ -helix region of gp120 served as positive and negative controls, respectively. **C** Peptides of the  $\beta$ -strands in HIV-1 MN gp120 increased infection with HIV-1 SF162 in a dose-dependent manner. The results are presented as the fold change in the enhancement relative to that measured in the absence of peptide. The numbers indicate peptide numbers. The data are presented as the mean ( $\pm$ S.D.) of three experiments. **D** The ability of peptides derived from  $\beta$ -strand and  $\alpha$ -helix regions in gp120 to increase HIV-1 infectivity was compared. **E** Schematic description of the experimental procedure

are the main secondary structures of gp120 and the shared motif of amyloid fibrils. Interestingly, EPs are located in  $\beta$ -strands 19 and 20 in gp120. A shorter form of EP1, identified in gp120-treated rat hepatocytes, can form amyloid fibrils that increase HIV-1 infectivity [21, 22]. These findings suggest that some natural gp120-releasing amyloidogenic peptides or amyloids might exist. Thus, it is worth studying the natural occurrence of gp120-derived amyloid fibrils and their physiological relevance to HIV-1 pathogenesis in vivo.

In this study, a peptide array was first constructed to scan for overlapping peptides covering the entire length of gp120. This screen was designed to provide insight into the ability of  $\beta$ -strands in HIV-1 gp120 to form amyloid fibrils and, in turn, boost HIV-1 infectivity. Next, the presence of gp120-derived amyloidogenic peptides (GAPs) and amyloids was demonstrated in the products of enzyme-treated gp120 and HIV-1 infectivity samples in vitro. The biochemical function of these gp120-derived amyloid fibrils was also studied. Finally, in vitro findings were confirmed in the lymphatic fluid, lymph nodes (LNs) and cerebrospinal fluid (CSF) of AIDS patients ex vivo or in vivo. The results from these studies support the existence of a novel function of gp120-derived

infection-promoting amyloid fibrils in viral pathogenesis and suggest a new target for antiretroviral treatment.

## RESULTS

### Peptides derived from the $\beta$ -strands of HIV-1 gp120 form amyloid fibrils that increase the infectivity of the HIV-1 virus clone

In addition to EPs derived from strands  $\beta$ 19 and  $\beta$ 20 in gp120 [17], as noted above, we investigated whether  $\beta$ -strands in gp120 could form amyloid fibrils that are able to increase HIV-1 infectivity. For this purpose, we used an HIV-1 MN Env peptide set comprising a series of synthetic peptides (15-mers) covering the full length of the HIV-1 MN envelope with a 4-amino acid shift for each peptide. The protein gp120 contains 30  $\beta$ -strands, 6 helices and undefined structures (Fig. 1A). The peptides were first aligned with the secondary structure (PDB code 3JWD), as indicated in previous reports [19, 20, 23], via PyMOL. Then, 60 peptides derived from  $\beta$ -strands, 13 peptides derived from  $\alpha$ -helices and 6 peptides covering both  $\beta$ -strands and  $\alpha$ -helices from the peptide set were used for primary screening (Table S1).

Twenty-nine peptides that might form amyloid fibrils, as indicated by the increased fluorescence intensity upon binding to thioflavin T (ThT,  $\geq 40$  units, approximately 50% greater than that of the solvent control), were identified [24]. All these amyloid-forming peptides were derived from  $\beta$ -strands in gp120, including strands  $\beta 3'$ ,  $\beta 4'$ ,  $\beta 1$ ,  $\beta 3$ ,  $\beta 9$ ,  $\beta 11$ ,  $\beta 12$  and  $\beta 16$ -23 (Table S1).

Next, the fibrillary morphology of these  $\beta$ -strand fragments was examined via transmission electron microscopy (TEM). Many of these peptides had fibrillary structures, despite minor differences in shape. Amyloid fibrils formed by several peptides, such as 6257, 6303, and 6314, displayed straight, long, rigid, and unbranched structures, similar to those of SEVIs (semen-derived enhancers of viral infection), which are naturally occurring amyloid fibrils in human semen [14, 25]. Interestingly, amyloid fibrils formed by fragments, such as 6217, 6281, and 6313, appear to consist of short, soft, thin structures (Fig. 1B). None of the peptides derived from the  $\alpha$ -helices of gp120 formed amyloid fibrils (Fig. 1B and Table S1).

Since amyloid fibrils can increase HIV-1 infectivity [14, 17], a CCR5-tropic clone virus was used to test whether these amyloid fibrils from the  $\beta$ -fragments in gp120 could also boost HIV-1 infectivity. Strikingly, many (34 out of 60) peptides derived from gp120  $\beta$ -strands significantly increased HIV-1 infectivity by 1- to 216-fold (Fig. 1C and Table S1). Some of these peptides mediated a stronger effect than did EPs (Fig. 1C). In sharp contrast, most fragments from the  $\alpha$ -helix region showed no signs of fibril formation or enhancement of HIV-1 infectivity. Two peptides overlapping  $\beta$ -strand and  $\alpha$ -helix structures, namely, 6301 and 6305, exhibited moderate increases in infectivity (Fig. 1D and Table S1). Interestingly, an amyloidogenic peptide derived from the spike protein of SARS-CoV-2 also increased HIV-1 infectivity (Fig. S1a). Overall, the peptidic formation of amyloid fibrils in gp120 correlated with increased HIV-1 infectivity (Fig. S1b), suggesting that the formation of amyloid fibrils by the fragments of  $\beta$ -strands in gp120 is essential for the enhancement of HIV-1 infectivity.

According to in vitro peptide library screening, most  $\beta$ -strands in gp120 can form amyloid fibrils that are capable of driving HIV-1 infection. These peptides derived from  $\beta$ -strands in gp120 are henceforth termed GAPs, and the amyloid fibrils formed by GAPs are hereinafter denoted gp120-derived enhancers of viral infection (GEVIs). It was hypothesized that GAPs and GEVIs might occur naturally to facilitate HIV-1 infection. To test this hypothesis, the presence of GAPs and GEVIs was confirmed in the enzymatic degradation products of gp120, in in vitro-generated conditioned viral infection samples, and in in vivo-generated lymphatic fluid, as well as in the LNs and CSF of AIDS patients. The biochemical properties and functionality of GAPs and GEVIs were also studied (Fig. 1E).

### GAPs and GEVIs occur after enzymatic digestion of gp120 in vitro

Tissue fluid, plasma and lymph contain abundant enzymes. Free gp120 might be proteolyzed by enzymes in vivo to produce GAPs and GEVIs. Therefore, the presence of GAPs or GEVIs was determined after the exposure of gp120 to three enzymes: thrombin B [26], fucosidase (AFU) [27], and plasmin. After exposure to each enzyme, HIV-1 gp120 was gradually degraded (Fig. S2). LC-MS/MS analysis was applied to identify peptide fragments smaller than 3 kDa among the degradation products. Gp120 was cleaved by each enzyme, generating fragments of multiple sizes (Table S2). Many peptides were derived from the  $\beta$ -strand structures, predominantly  $\beta$ -10, -13, -14, -20, -21, -22, -23, and -25. Several representative peptides were selected for chemical synthesis and characterized according to their biochemical function (Fig. 2A). Most of the selected peptides were found to form turbid solutions when dissolved in PBS or first in DMSO followed by dilution in PBS, suggesting that they can spontaneously form amyloid fibrils. Most

of these GAPs displayed  $\beta$ -sheet structures, as revealed by circular dichroism (CD) (Fig. 2B). Accordingly, these GAPs also bound to the amyloid-specific probes Congo red (Fig. 2C) and ThT (Fig. 2D) in a dose-dependent manner. As observed by TEM, all these synthetic GAPs could form amyloid fibril structures (Fig. 2E). Notably, amyloid fibrils were observed by TEM in all mixtures of enzyme-treated gp120, whereas the control of each enzyme or gp120 had no amyloid structures (Fig. 2G).

Most of the amyloid fibrils formed by these enzyme-releasing GAPs also increased HIV-1 infectivity and some even induced more pronounced increases in infectivity than did EP2 (Fig. 2F). Taken together, these results suggest that the enzyme-triggered proteolysis of gp120 results in the production of GAPs and GEVIs.

### GAPs and GEVIs exist in the culture medium of HIV-1-infected cells in vitro

To validate these findings in a more complex biological system, the presence of GAPs and GEVIs was investigated in the culture medium of HIV-1-infected cells in vitro. MT-2 cells and CEMx 174 5.25 M7 (CEMx M7) cells were infected with HIV-1 IIIB (X4-tropic) and HIV-1 SF162 (R5-tropic), respectively. Peptide fragments smaller than 3 kDa were collected from viral supernatants seven days post-infection and analyzed by LC-MS/MS. Two GAPs, namely, GAP380-396 in samples of HIV-1 SF162-infected CEMx M7 and GAP230-244 in samples of HIV-1 IIIB-infected MT-2, were detected (Fig. 3A, and Fig. S3a, b). Chemically synthesized GAP380-396 and GAP230-244 had typical  $\beta$ -sheet structures, as revealed by CD (Fig. 3B). Both peptides bound to the amyloid dyes ThT (Fig. 3C) and Congo red (Fig. 3D) and formed amyloid fibrils, as observed by TEM (Fig. 3E). As expected from the above results, amyloid fibrils formed by these two GAPs could increase infection by CCR5-tropic HIV-1 SF162 (Fig. 3F), CXCR4-tropic HIV-1 NL4-3 (Fig. 3G) and dual-tropic 81A and NL4-3 (Fig. 3H).

To confirm by confocal microscopy whether GEVIs spontaneously formed during viral infection, Proteostat<sup>®</sup> and ThT dyes were employed to stain amyloid fibrils in the supernatant of infection samples. Strikingly, fluorescent amyloid structures were detected in both infection samples (Fig. S3c), while the control culture medium produced only a limited fluorescence signal, strongly suggesting that infection-promoting amyloid fibrils naturally exist. Furthermore, a polyclonal antibody against gp120, which reacts with several  $\beta$ -fragments in gp120 (Fig. S3d, e), colocalized with Proteostat signals (Fig. 3I, J), demonstrating that infection-promoting GEVIs formed during viral infection.

To verify the findings obtained with confocal microscopy, immuno-TEM was applied to directly visualize individual fibrils via high-resolution imaging. The infection samples contained mature fibrils that could be partly stained with an immunogold-labeled gp120 antibody (Fig. 3K). However, the immunogold-labeled antisera did not recognize amyloid fibrils, confirming the presence of GEVIs in response to infection challenges.

### Ability of GEVIs to increase HIV-1 infectivity and their mechanism of action

GAP380-396 and GAP230-244, found in viral infection samples, were used to study the ability of GEVIs to promote HIV-1 infection. Fibrils formed by both GAPs increased the infectivity of R5-, X4-, and dual-tropic HIV-1 clones in TZM-bl cells at concentrations  $\geq 0.625$   $\mu$ M (Fig. 3F-H). GEVI also increased the infectivity of laboratory-adapted HIV-1 IIIB and a panel of primary HIV-1 strains tested in TZM-bl cells (Fig. 4A). Consistent with previous findings [14], the most dramatic effects were obtained for infection with low viral doses (Fig. S3f). In addition to using TZM-bl, a reporter cell line for a single-cycle infection, the ability of GEVIs to increase HIV-1 infectivity was also tested in lymphocytes that allow multiple-cycle infection. As expected, GEVIs also promoted HIV-1 IIIB infection in MT-2 cells (Fig. 4B) and HIV-1 SF162 infection in CEMx M7 cells (Fig. 4C). Notably, different GEVIs mediated distinct

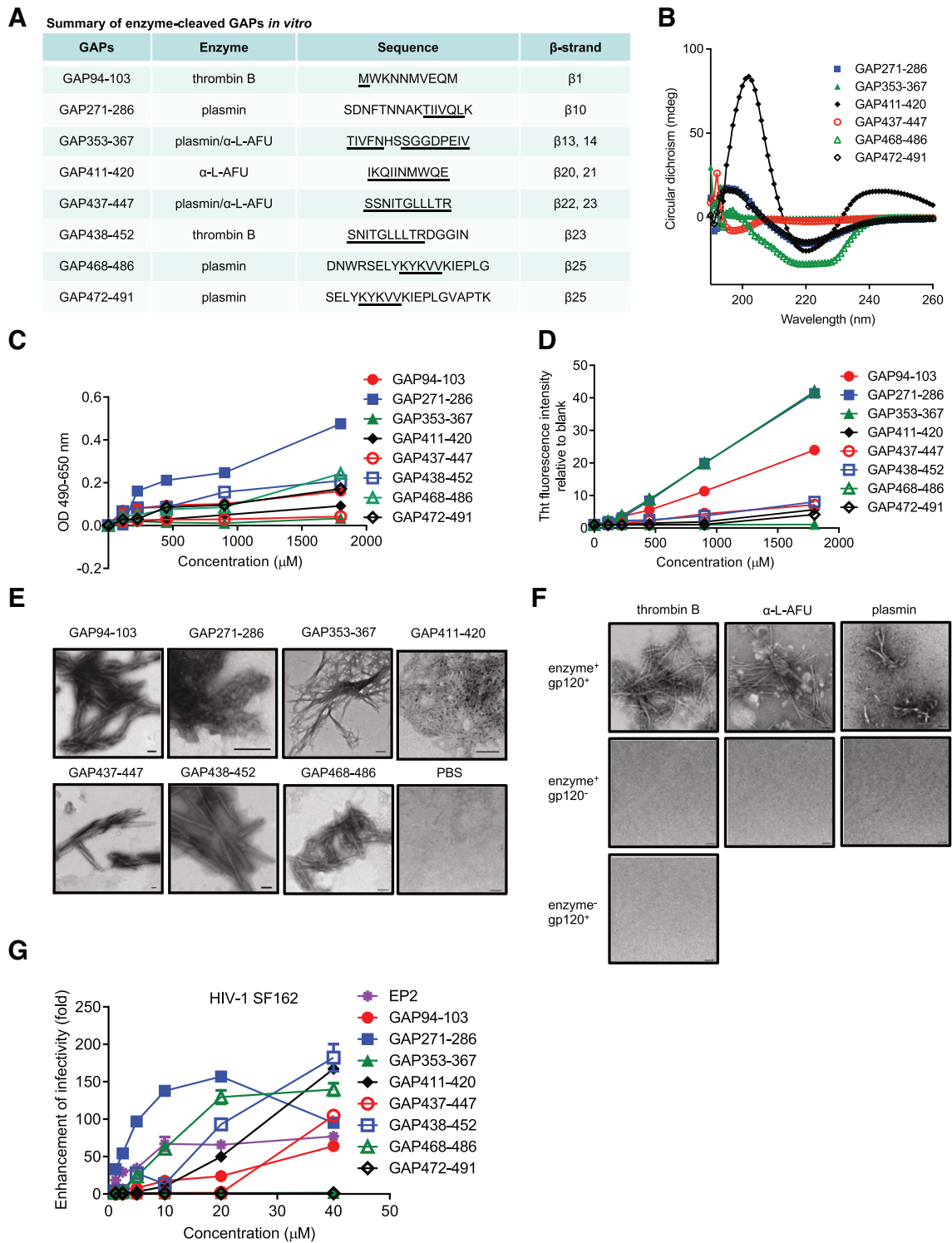


**Fig. 2** Degradation of gp120 in the presence of physiological enzymes releases *in vitro* GAPs that form amyloid fibrils and increase HIV-1 infectivity. **A** Selected GAPs found among enzyme-mediated degradation products *in vitro*. The numbers correspond to the amino acid positions in full-length gp120. **B** CD spectroscopic analysis of the  $\beta$ -sheet structures of different GAPs. The final peptide concentration was 150  $\mu$ M. The experiment was repeated once, and a similar result was obtained. GAPs bind to two specific amyloid fibril dye, including Congo red (**C**) and ThT (**D**), in a dose-dependent manner. The results are presented as the mean  $\pm$  S.D. of three experiments. **E** Transmission electron micrographs of amyloid fibrils formed by different GAPs. The scale bars indicate 200 nm for each image. **F** The enhancement of HIV-1 SF162 infection by GAPs was determined in TZM-bl cells and is shown relative to that measured in the absence of peptide. The data represent the mean values of triplicate measurements from one of three independent experiments that yielded similar results. **G** Endogenous amyloids in gp120-treated with thrombin, AFU or plasmin were detected via TEM. Each enzyme and gp120 set were used as controls. The scale bars indicate 100 nm for each image

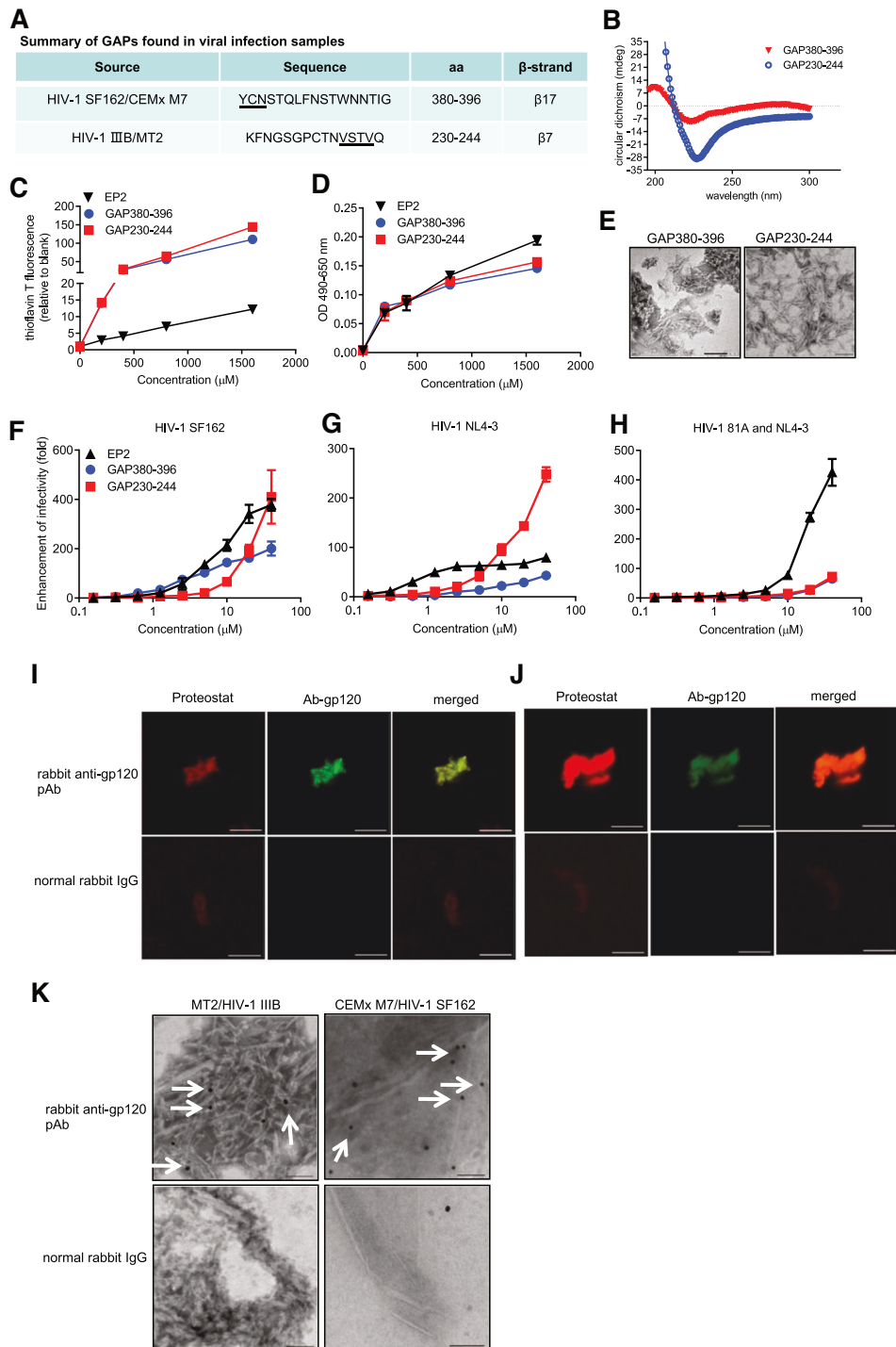


**Fig. 3** GAPS and GEVIs are found in the viral infection supernatant. **A** Sequence of GAPS found in the supernatant of the viral infection system. **B**  $\beta$ -Sheet formation in GAP380-396 and GAP230-244 solutions monitored by CD analysis. The experiment was repeated once, and a similar result was obtained. Measurement of GAP380-396 and GAP230-244 with the amyloid-binding agents ThT (**C**) and Congo red (**D**). The data are presented as the mean  $\pm$  S.D.s ( $n = 3$ ). **E** Electron micrographs of fibrils formed by GAP380-396 and GAP230-244. The scale bars indicate 200 nm for each image. Fibrils formed by GAP380-396 and GAP230-244 increased the infection of TZM-bl cells by R5-tropic HIV-1 SF162 (**F**), X4-tropic HIV-1 NL4-3 (**G**), and dual-tropic HIV-1 81A and NL4-3 (**H**). Virions pretreated with GEVI at the indicated concentrations for 5 min were used to infect TZM-bl cells. The cells were assayed for luciferase activity 48 h post-infection. The results indicate an  $n$ -fold increase in infectivity relative to infection in the absence of fibrils. The mean ( $\pm$ S.D.) values of triplicate measurements from one of three independent experiments yielded similar results. (**I**, **J**) A polyclonal anti-gp120 antibody recognizes infection-generated GEVI fibrils in vitro. Supernatants from HIV-1 IIIB-infected MT-2 cells (**I**) and HIV-1 SF162-infected CEMx M7 cells (**J**) were incubated with pAb-gp120 (upper panel) or control rabbit IgG (lower panel). The amyloid/antibody complexes were then pelleted, washed, and detected using a FITC-labeled secondary antibody (green). All samples were subsequently costained with amyloid-specific Proteostat dye (red). The scale bar represents 20  $\mu$ m. **K** Immunogold labeling of infection-generated GEVI fibrils. Transmission electron micrographs of viral infection supernatants treated with pAb-gp120 (upper panel) or control rabbit IgG (lower panel), which were used as primary antibodies, and gold-conjugated anti-rabbit secondary antibodies. Scale bar, 100 nm. The white arrows indicate gold particles bound to amyloid fibrils

patterns of increased infection by different viral strains in various cell lines. Viral properties and fibrillary properties, such as binding ability and fibril structure, might also influence the ability of GEVIs to increase HIV-1 infectivity. GEVIs mediated increased viral infection irrespective of the viral phenotype, genotype, or cell type.

In examining the infection-generating mechanism of GEVIs, the supernatant of a GEVI solution did not promote HIV-1 infectivity, whereas the pellet portion of GEVI was highly active (Fig. 4D). This observation suggested that mature fibrils, not monomeric peptides, were responsible for increasing HIV-1 infectivity. Using a virus removal assay [17], GEVI was shown to increase HIV-1 infectivity only when peptides were added to cells either before or at the same time as viruses attached to cells. Limited postentry enhancement of HIV-1 infectivity was detected when peptides were added after virions had bound to target cells (Fig. 4E). Therefore, it was concluded that GEVIs target the viral entry process to boost virus infection.

To understand how GEVIs exert their pathogenic influence on HIV-1 infectivity, a virus pull-down assay [17] was used for a closer examination of the mechanism of action. The infectivity of HIV-1 treated with GEVI or EP pellets was markedly greater than that viruses treated with PBS (Fig. 4F). Moreover, higher viral infectivity was detected (Fig. 5G) in TZM-bl cells preincubated with GEVIs. The next logical step was a closer examination of the binding properties of GEVIs with viruses and target cells. For this purpose, we incubated Proteostat-stained GEVI with eGFP-labeled HIV-1 virions in the presence or absence of TZM-bl cells. Fluorescence microscopy revealed that the GEVIs formed by GAP380-396 (Fig. 4H, upper panels) and GAP230-244 (Fig. S4a, upper panels) interacted extensively with HIV-1 virions. Three-color imaging of fibrils, virions, and cells demonstrated that the fibrils promoted attachment of the virions to the target cells (Figs. 4H, S4a, lower panels).

The zeta potential further showed that different GEVIs form amyloid fibrils with distinct surface electrical properties. Fibrils formed by GAP230-244, for instance, show a positive zeta potential, similar to that of SEVIs [28]. In contrast, the fibrils of GAP380-396 display a negative zeta potential, while those of EP2 exhibit dielectric properties (Fig. S4b). Cellulose sulfate, a polyanion with negative charges, markedly decreased the enhancement of viral infectivity mediated by GAP230-244 and SEVIs, which have positive zeta potentials, but had only negligible effects on EP2, which has a neutral zeta potential, and on the fibrils of GAP380-396, which has a negative zeta potential (Fig. S4c). The positively charged lysine residue might be a key residue for the ability of GAP230-244 to increase HIV-1 infectivity [28]. In contrast, the ability of the fibrils formed by GAP380-396 to increase HIV-1 infectivity was weakened in the presence of polybrene, a cationic polymer that neutralizes the charge repulsion between virions and the cell surface, thereby increasing infectivity (Fig. S4d). The presence of the hydrophobic amino acid residue Trp in EP2 may facilitate hydrophobic interactions between amyloids and the viral membrane and promote the embedding of fibrils into the cell membrane, thus increasing viral infection rates [29]. These results suggested that GEVIs promote viral attachment to target cells via their surface electrostatic properties.

In summary, these data indicate that the studied  $\beta$  fragments in gp120 can spontaneously form amyloid fibril structures and that, upon dissolution or dilution of the peptide, the protein can readily bind to the amyloid fibril-specific dye ThT (Fig. S4e), implying spontaneous  $\beta$ -sheet formation.

#### GEVIs suppressed the anti-HIV-1 activity of antiretroviral drugs (ARVs)

The anti-HIV-1 activity of several ARV-based microbicides was impaired in the presence of certain HIV-1 infectivity-enhancing factors, such as SEVIs and semen [30, 31]. To evaluate whether GEVIs can also counteract the inhibitory effect of current clinically

available ARVs, we tested the effects of GAP380-396 and GAP230-244 on the antiviral activity of four classes of ARVs, namely, entry inhibitors, non-nucleoside reverse transcriptase inhibitors (NNRTIs), nucleoside reverse transcriptase inhibitors (NRTIs) and integrase inhibitors against infection by HIV-1 SF162. Surprisingly, all the tested ARVs showed reduced anti-HIV-1 activity in the presence of 1  $\mu$ M GAPs (Table 1). This low concentration of GAPs generally decreased the in vitro effectiveness (i.e., increased the IC<sub>50</sub> value) of the ARVs by ~1.0- to 14.8-fold. However, the peptide from the  $\alpha$ -helix region in gp120 had no effect on the antiviral activity of the ARVs (Table S3). This raises the concern that the presence of GEVIs in HIV-infected patients may markedly decrease the in vivo efficacy of antiretroviral therapy.

#### Different GAPs coaggregate to form heterologous amyloid fibrils

The copolymerization of different amyloid sequences has been shown to occur in several amyloid deposition-related diseases [32, 33]. Because of their specific characteristics, GAP variants might coassemble and thereby compound the pathogenic in vivo consequences. To test this hypothesis, we chemically synthesized and analyzed three fluorescently labeled GAPs, FITC-GAP230-244 (green), Rho-GAP380-396 (red), and MCA-EP2 (blue). All peptide solutions were turbid and displayed the characteristic signals of  $\beta$ -sheet structures (Fig. 5A). In addition, all three fluorescently labeled GEVIs displayed typical fibrillary morphologies, as evidenced by TEM (Fig. 5A, inserted panels). Therefore, it was established that fluorescently labeled GAPs can form amyloid fibrils.

Next, two peptides were simultaneously dissolved (at an equal molar ratio) to allow cross-reaction. The newly formed heterologous fibrils bound to ThT and Congo red (Fig. S5). After mixing two or three fluorescently labeled GAPs at a molar ratio of 1:1 or 1:1:1, characteristic thread-like fibrillar shapes were detected in each mixed sample by TEM (Fig. 5B). Two- or three-color confocal imaging permitted the visualization of different colocalized GAPs within the same amyloid deposit (Fig. 5B).

The evaluation of heterologous fibrils showed that the divergent GEVIs had comparable ability to increase HIV-1 infectivity to that of the homogeneous GEVIs (Fig. 5C). Interestingly, GAP380-396 and EP2 formed heterologous fibrils with the capacity to induce even more pronounced infectivity than homogeneous fibrils (Fig. 5C). It remains to be investigated whether coaggregation alters the properties of heterologous fibrils compared to those of homogeneous fibrils in the context of heightened HIV-1 infectivity. In addition, heterologous fibrils with different fluorescent signals within a single fibril should be further visualized by two-color superresolution microscopy.

#### GAPs and GEVIs occur in the lymph tissue of HIV-1/AIDS patients

The physiological presence of GAPs and GEVIs in AIDS patients was subsequently examined. Plasma from HIV-1-positive patients was assessed first, but no peptide sequence of gp120 was observed, possibly because the highly abundant serum proteins interfered with the detection of low-abundance peptides. Since LNs are the major location for viral infection and latency, lymphatic leakage was evaluated in an advanced AIDS patient with cervical carcinoma (Table S4). A peptide derived from gp120, which covered  $\beta$ 14,  $\beta$ 15, GAP354-369 (Fig. 6A and Fig. S6a), was identified, as was one derived from gp41 (data not shown). Synthetic GAP354-369 showed evidence of fibril formation in vitro, as indicated by an increase in fluorescence and absorbance upon binding to ThT and Congo red, respectively (Fig. 6B), a characteristic signal of  $\beta$ -sheet structures by CD (Fig. 6C), and by the observation of characteristic fibrillar structures by TEM (Fig. 6C, inserted panel). Fibrils formed by GAP354-369 also increased infection by R5-, X4- and dual-tropic HIV-1 clones in TZM-bl cells (Fig. 6D).

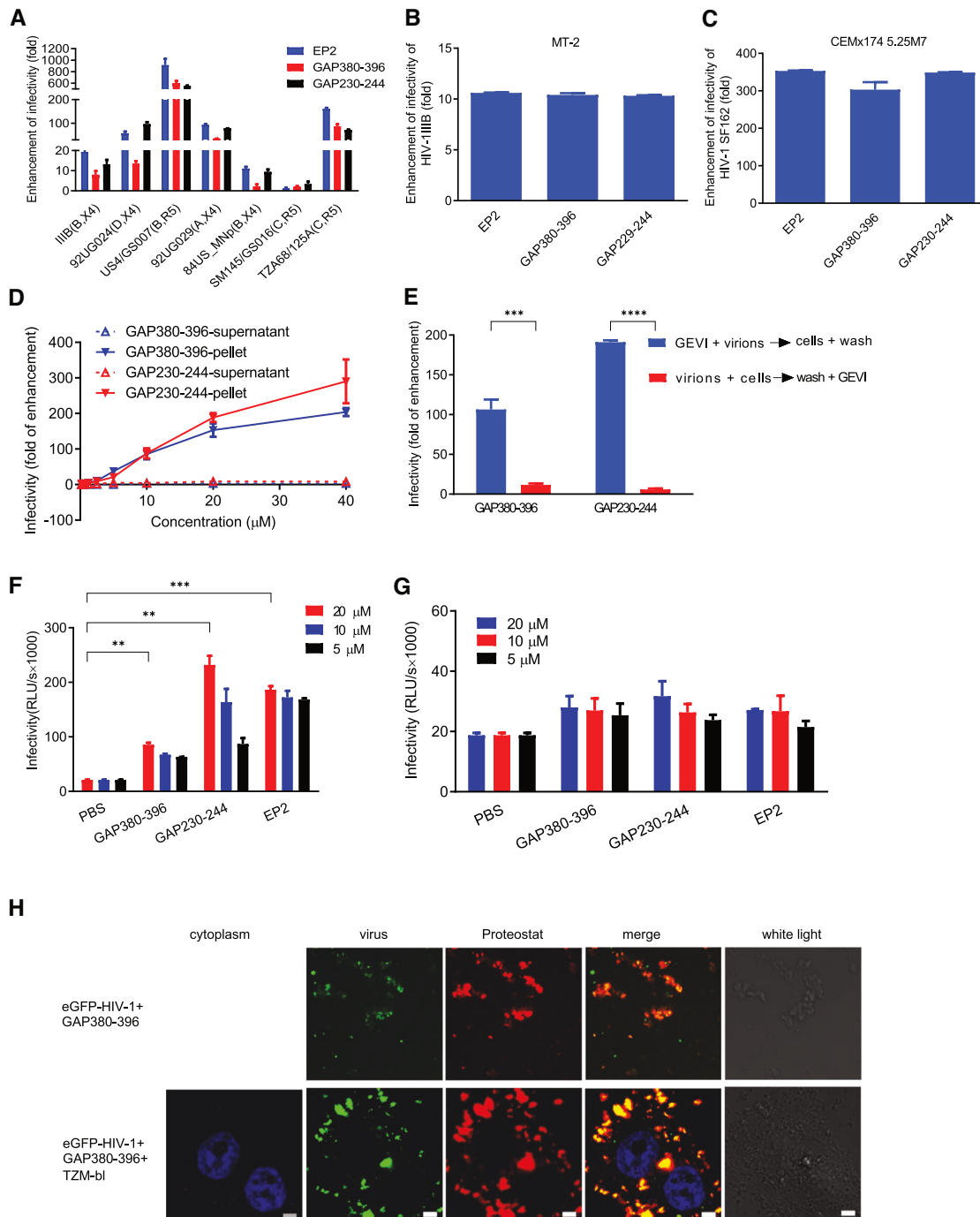


**Fig. 4** GEVI-induced increases in the infectivity of different HIV-1 clinical isolates and the mode of action of GEVIs. **A** Relative effect of GAP380-396 and GAP230-244 (10  $\mu$ M) on the infection of T2M-bl cells by various HIV-1 clinical isolates. The subtypes (clades) and biotypes (coreceptor tropisms) of the viral isolates are indicated. The results indicate n-fold infectivity enhancement relative to infection in the absence of fibrils. The mean ( $\pm$ S.D.) of all three measurements is shown. GAP380-396 and GAP230-244 at 10  $\mu$ M increased the infection of HIV-1 IIIB and SF162 in MT-2 cells (**B**) and CEMx M7 cells (**C**), respectively. The n-fold increase in the infectivity and the mean ( $\pm$ S.D.) of the three measurements are shown. **D** Increased HIV-1 SF162 infectivity via the formation of amyloid fibrils. Peptide solutions of each GAP were centrifuged at 12,000 rpm for 10 min. The supernatant, containing soluble peptide, or the pellet, which represents insoluble fibrils, was applied to infected T2M-bl cells. The results shown are representative of three independent experiments. The final concentration of GAPs was 10  $\mu$ M. **E** GEVIs increase HIV-1 infectivity by targeting the viral entry process. The results shown are representative of three independent experiments. **F** GEVIs bind to virions to increase HIV-1 infectivity. HIV-1 bound to GEVI fibrils in the pellets was used to infect T2M-bl cells. Infections were determined via a luciferase assay. The results shown are the mean ( $\pm$ S.D.) of three independent experiments. **G** GEVI fibrils bind directly to target cells to increase HIV-1 infectivity. GEVI was first incubated with T2M-bl cells and subsequently washed with medium. The viruses were added and incubated at 37  $^{\circ}$ C for 2 h. The medium was changed, and infections were confirmed 48 h later. The data are presented as the mean ( $\pm$ S.D.) of three independent experiments. **H** EGFP-labeled HIV-1 SF162 particles (green) were added to Proteostat-stained GAP380-396 amyloids (red) and T2M-bl cells (blue) and imaged by confocal microscopy. Results are from one of two independent experiments yielded similar results. Scale bar = 20  $\mu$ m.  $p < 0.05$  was considered to indicate statistical significance. Two-way ANOVA was used for Statistical analysis

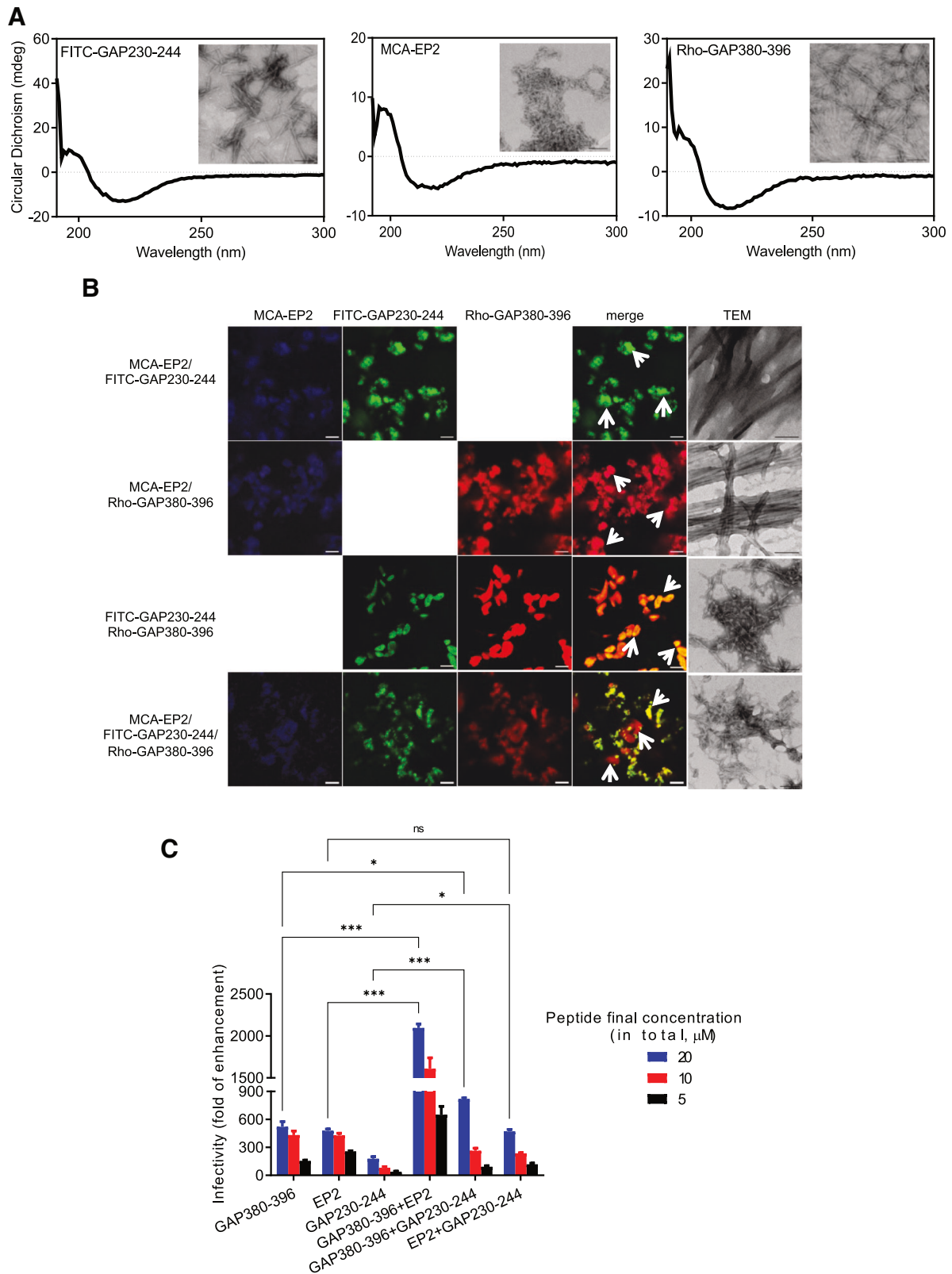


**Fig. 5** Different GAPs form heteroamyloid fibrils. **A** Fluorescently labeled GAPs (10  $\mu$ M) display typical  $\beta$ -sheet structures, as shown by CD. The inset graphs are electron micrographs of fluorescently labeled GAPs (10  $\mu$ M). Left panel: FITC-GAP230-244 (green); center panel: MCA-EP2 (blue); right panel: Rho-GAP380-396 (red). Scale bar = 200 nm. **B** GAPs cross-interact and form heteroamyloid fibrils. Different GAPs were mixed at an equal molar ratio (100:100  $\mu$ M). The samples were then centrifuged, and the pellets were subjected to confocal microscopy. The scale bars represent 20  $\mu$ m. TEM images are also shown. Scale bar = 200 nm. **C** Increased expression of HIV-1 SF162 infection by heteroamyloid fibrils and homoamyloid fibrils. The mean values ( $\pm$ S.D.) of triplicate samples from one of three independent experiments that yielded similar results are shown.  $p < 0.05$  was considered to indicate statistical significance. Two-way ANOVA was used for statistical analysis



**Table 1.** Effect of GEVI on the antiviral activity of ARVs against infection of HIV-1 SF162<sup>a</sup>

Category and drugs		IC <sub>50</sub> (nM) for inhibiting HIV-1 SF162 (R5) infection				
		+ PBS	+ GAP380-396 <sup>b</sup>	Fold increased	+ GAP230-244 <sup>b</sup>	Fold increased
Entry inhibitors	Maraviroc	6.18 ± 0.53	14.02 ± 2.00	1.3	12.12 ± 1.32	1.0
NRTIs	Emtricitabine	375.55 ± 73.63	1117.49 ± 126.78	2.0	469.05 ± 75.05	1.2
NNRTIs	TMC120	1.24 ± 0.032	16.98 ± 0.33	12.7	19.65 ± 0.24	14.8
	Nevirapine	19.21 ± 4.56	78.86 ± 3.75	3.1	66.49 ± 15.12	2.5
	Efavirenz	7.59 ± 0.56	14.94 ± 2.47	1.0	10.97 ± 1.36	1.4
Integrase inhibitors	Raltegravir	47.49 ± 12.65	126.65 ± 11.12	1.7	193.59 ± 11.07	3.1

<sup>a</sup>Abbreviations: IC<sub>50</sub> 50% inhibitory concentration, NRTIs nucleoside reverse transcriptase inhibitors, NNRTIs non-nucleoside reverse transcriptase inhibitors, TMC120 dapivirine. Gaps were tested at 1 μM

<sup>b</sup>Data are the means of triplicate measures, and the experiment was repeated once. A representative set of data is shown

Proteostat-positive amyloid fibrils were also found to be involved in lymphatic leakage from an AIDS patient based on the polyclonal anti-gp120 antibody, which recognizes structures involved in lymphatic leakage via the use of an amyloid probe (Fig. 6E). To confirm the fibrillar nature of the structures recognized by Proteostat and anti-gp120, TEM was performed on lymphatic fluid treated with immunogold-labeled anti-gp120. As shown in Fig. 6F, gold-conjugated anti-gp120 antibodies specifically bound to mature fibrils in lymphatic fluid but failed to recognize control rabbit IgG.

Importantly, when we tested the ability of lymphatic fluid from an AIDS patient to enhance HIV-1 infectivity toward TZM-bl cells, we found that inactivated lymphatic fluid could increase HIV-1 infectivity in a dose-dependent manner and that whole lymphatic fluid could increase HIV-1 infectivity by 3.5-fold (Fig. 6G). These data provide evidence that Gaps and GEVIs occur naturally in lymphatic leakage in AIDS patients and that lymphatic leakage could increase HIV-1 infectivity.

To further confirm the potential localization of the GEVI in vivo, we performed Congo red/immunohistochemistry double staining (Fig. 6H) and amyloid/gp120/nuclear immunofluorescence triple staining (Fig. S6b) [34, 35] of LNs from HIV/AIDS patients (Table S5). The results showed that gp120 was clearly expressed in the cytoplasm and extracellular space, while Congo red and Proteostat were observed in the extracellular space (Fig. 6H). Arrowheads indicate the colocalized signals of gp120 and amyloid (Fig. 6H and Fig. S6b).

### GEVIs and Gaps occur naturally in the CSF of HIV-1/AIDS patients

HIV-1 infects the central nervous system (CNS), and brain tissue is a reservoir for viral persistence. Therefore, HIV-1 is found in the brain parenchyma (microglia, astrocytes, oligodendrocytes and neurons) and cerebrospinal fluid (CSF). Soluble gp120 has been detected in the CSF of AIDS patients with a low blood viral load [36]. Experiments were therefore performed to detect the presence of Gaps/GEVIs in the CSF. CSF samples were collected from healthy volunteers and HIV-1/AIDS patients receiving antiretroviral treatment (ART) for TEM analysis (Table S6). Notably, amyloid fibrils were detected in the CSF of AIDS patients. As shown in Fig. 7A, pathological aggregation or tangling of amyloid fibrils was observed in the CSF of one AIDS patient. To further verify the presence of GEVIs/Gaps in the brain, LC-MS/MS analysis of the CSF of HIV-1-positive patients was subsequently carried out (Fig. S7a). Peptides from various gp120 regions of different HIV-1 strains were identified (Fig. 7B). The four samples shared some common peptide sequences (Fig. 7B and Table S7). Moreover, Gaps or homologous sequences of Gaps identified in the above study were also found in CSF samples from one or more HIV-1-positive patients (Fig. S7b–d and Table S8).

The biochemical properties of Gaps identified in CSF from AIDS patients were further confirmed. One representative peptide,

GAP196-209, which was highly abundant in CSF samples (Fig. 7C, D) from all four AIDS patients, was selected. Synthetic GAP196-209 spontaneously formed mature amyloid fibrils (Fig. 7E), and its fibrillary form could bind with Congo red (Fig. 7F). CD spectroscopy showed a negative peak at 217–218 nm and a strong positive peak at 195–198 nm, indicating a typical β-fold structure (Fig. 7G). TEM revealed that GAP196-209 had a typical amyloid fibril shape (Fig. 7H). GAP196-209 fibrils also promoted the infection of TZM-bl cells (Fig. 7I, J) and human glioblastoma U87 cells (Fig. S8) by HIV-1 SF162 and HIV-1 NL4-3. These findings support the relevance of the natural presence of Gaps/GEVIs in the CNS of AIDS patients.

### DISCUSSION

In the present study, a novel function of free gp120 in vivo is proposed. Specifically, it is hypothesized that gp120, upon proteolysis, releases biologically active amyloidogenic fragments (Gaps) that form amyloid fibrils (GEVIs) to increase HIV-1 infectivity. By screening a peptide library of gp120, most β-strand fragments in gp120 that can form amyloid fibrils were identified. Interestingly, these Gaps and GEVIs were found to occur naturally in vitro in enzymatic degradation and in HIV-1 infection samples, as well as in vivo in lymphatic fluid, LN, and CSF samples from HIV/AIDS patients, based on mass spectrometry, TEM, immune-electron microscopy and double staining with primary antibodies binding to gp120-derived epitopes and amyloid-specific probes. These Gaps spontaneously formed β-sheet-rich amyloids, implying that amyloid-forming peptides can exert a biological effect on viral pathogenesis as soon as they are produced in vivo. Moreover, Andrey V et al. reported that longer peptides containing two or more β-strands may exhibit a greater propensity to form amyloid fibrils [37]. This finding is consistent with the present results because several peptides containing two β-strands showed a greater capacity to form amyloid fibrils and increase HIV-1 infectivity than peptides containing a single β-strand (Table 1; for example, 6217 vs. 6216, 6281 vs. 6280 and 6302 vs. 6301). As reported previously, EP3, which overlaps the sequences of both EP1 and EP2, showed a stronger ability to increase HIV-1 infectivity than either EP1 or EP2 alone [17]. As a result, the possibility that larger β-fragments derived from gp120 may exert a more profound impact on viral pathogenesis cannot be ruled out. Multiple GAP sequences are considered to play a role in viral pathogenesis. The β-fragment of gp120 that contributes the most to viral pathogenesis could not be defined because of unpredictable enzyme cleavage specificity, the likelihood of cleavage by more than one protease in vivo, and the variability of the gp120 sequence of different viral strains. Therefore, when generating specific antibodies to recognize Gaps or GEVI, an attempt was first made to raise antibodies against EP2 and GAP380-396 amyloid in rabbits. Unfortunately, neither antisera nor antibodies specific for the amyloid or monomeric forms of EP2 or

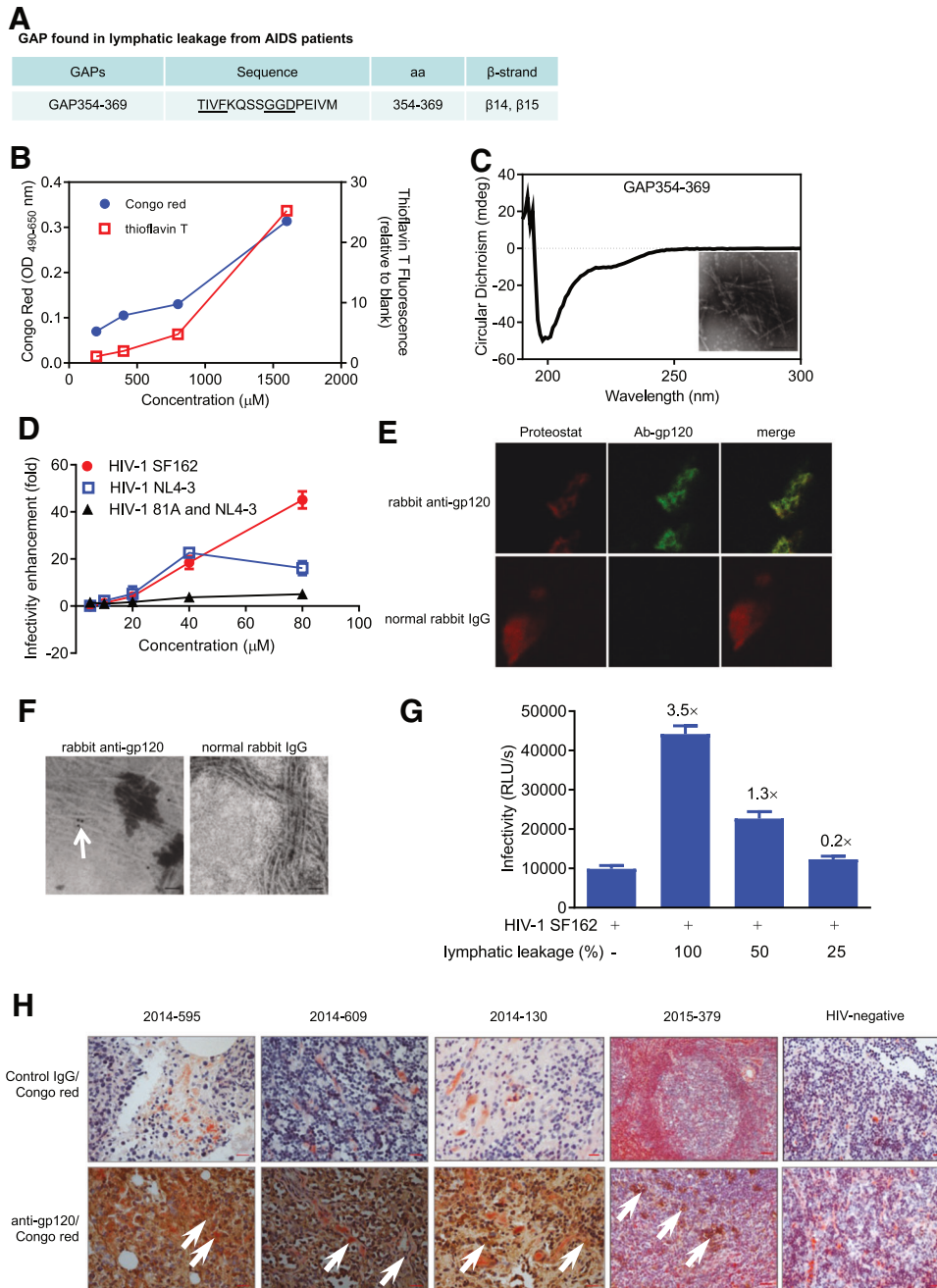


**Fig. 6** GAPs and GEVIs were detected in clinical lymphatic leakage and LNs from AIDS patients. **A** GAP sequences found during lymphatic leakage from AIDS patients. **B** Measurement of GAP354-369 expression in the presence of the amyloid-binding agents Congo red (blue, circular) and ThT (red, square). The mean values ( $\pm$ S.D.) of three independent measurements are shown. **C**  $\beta$ -Sheet formation by GAP354-369 (25  $\mu$ M) was monitored via CD analysis. The inserted panel shows a fibrillar image of GAP354-369 (10  $\mu$ M) obtained via TEM. Scale bar, 100 nm. **D** Fibrillar GAP354-369 enhanced HIV-1 infectivity in TZM-bl cells. The mean ( $\pm$ S.D.) of triplicate samples from one of three independent experiments that yielded similar results is shown. **E** Detection of lymphatic leakage by confocal microscopy using amyloid-specific Proteostat dye (red) and a rabbit anti-gp120 polyclonal antibody (green). **F** Immunogold labeling of endogenous gp120-derived amyloid fibrils during lymphatic leakage from AIDS patients. Transmission electron micrographs of lymphatic leakage fluid treated with rabbit anti-gp120 pAb or control rabbit serum as the primary antibody and gold-conjugated anti-rabbit secondary antibody. Scale bar, 20 nm. The white arrows indicate gold particles bound to amyloid fibrils. **G** Increased likelihood of HIV-1 SF162 infection by lymphatic leakage. The mean ( $\pm$ S.D.) of triplicate measurements of wells from one of two independent experiments yielded similar results. The numbers indicate the fold of the enhancement. **H** Paraffin-embedded LNs of AIDS patients were subjected to immunohistochemistry for detection using a control rabbit IgG (upper panels) or an anti-gp120 antibody (lower panels, brown), followed by Congo red staining for amyloid fibrils (red) and DAPI for nuclei (blue). The numbers indicate the number of HIV-1 patients. The samples were observed under a microscope. Gp120<sup>+</sup>/amyloid<sup>+</sup> staining is indicated by arrows. Scale bars = 20  $\mu$ m

GAP380-396 could be generated. Consequently, a specific antibody for each GAP could not be produced; instead, a polyclonal antibody against the whole gp120 was used. This polyclonal antibody recognized several  $\beta$ -fragments of gp120 in ELISA.

Although it also recognized intact gp120, the data showed gp120<sup>+</sup>/amyloid<sup>+</sup> double staining to exclude the interference of intact gp120. Potential GEVIs/GAPs that cannot be detected by this anti-gp120 antibody might also occur naturally. In addition to

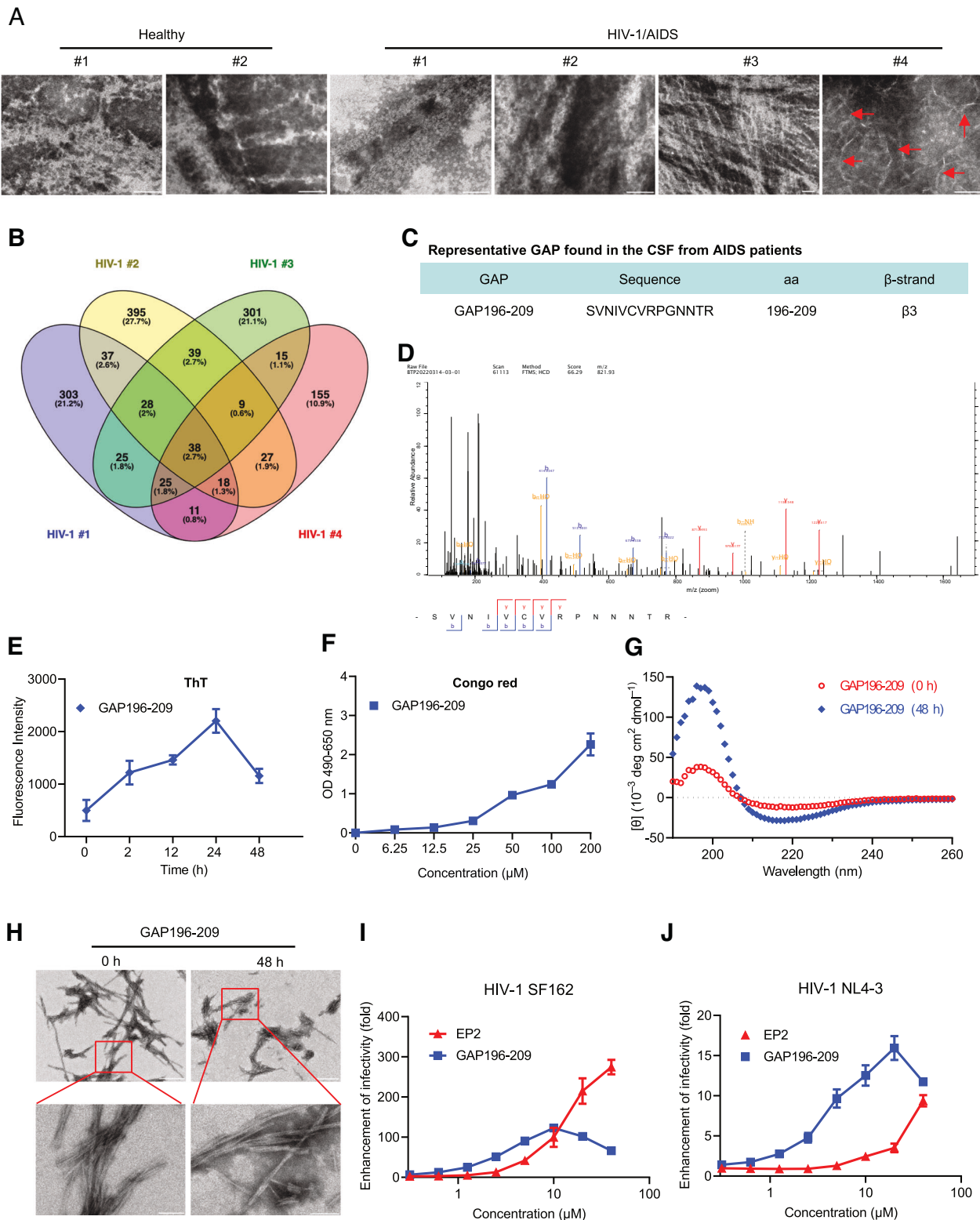


**Fig. 7** Detection of amyloid fibrils in the CSF of AIDS patients. **A** TEM micrographs of CSF collected from healthy individuals ( $n = 2$ ) and HIV-1<sup>+</sup> individuals ( $n = 4$ ). Amyloid fibrils are indicated with red arrows. The scale bar represents 100 nm. **B** Venn diagrams showing total GAPs found in CSF samples from the four HIV-1<sup>+</sup> patients identified by LC-MS/MS. **C** Representative sequence of GAP196-209 found in the CSF of four HIV-1<sup>+</sup> individuals. **D** Secondary spectrum of GAP196-209 identified by LC-MS/MS. **E** The fluorescent dye ThT was used to dynamically monitor amyloid fibril formation by GAP196-209 (50  $\mu$ M) within 48 h. The data are presented as the mean  $\pm$  S.D. from three independent measurements ( $n = 3$ ). **F** Measurement of GAP196-209 with the amyloid-binding agent Congo red. The data are presented as the mean  $\pm$  S.D. ( $n = 3$ ). **G**  $\beta$ -Sheet formation of GAP196-209 (30  $\mu$ M), as determined by CD analysis. **H** TEM micrographs of fibrils formed by GAP196-209 (200  $\mu$ M). Scale bar, 500 nm for the upper panels and 100 nm for the lower panels. The enhancement of HIV-1 SF162 (**I**) and NL4-3 (**J**) infectivity by GAP196-209 was determined in TZM-bl cells. The data represent the mean of triplicate measurements from one of three independent experiments that yielded similar results

self-assembly into amyloid fibrils to increase HIV-1 infectivity, these GAPs also cross-interact to form heterologous fibrils that display activity comparable to that of homogeneous fibrils in increasing HIV-1 infectivity. It was speculated that GAPs, like seminal amyloid fibrils, might also play a pathogenic role in promoting viral infection in vivo [14, 17]. Mechanistic studies revealed that GAP380-396 and GAP230-244 promoted HIV-1 infection by binding to the virus and target cells via their surface electrostatic properties.

Free gp120 may be shed from virions or released from HIV-1-infected cells as cell debris by cytopathic effects [38–40]. Over  $10^{10}$  virions are estimated to be generated per day. In light of the high replication activity and high turnover rate of HIV-1 in vivo [41, 42], relatively large amounts of gp120 are released in vivo. It was estimated that the concentration of soluble gp120 in the serum of HIV-1-infected individuals reached 960 ng/ml [43]. Released monomeric gp120 can be degraded into fragments by several proteolytic enzymes in vivo. An elevated proteolysis rate has been recorded in HIV-1-infected patients [44–46]. Catalytic antibodies can specifically degrade gp120 into small fragments in vivo [47–49]. Infected cells can also release fragments of gp120 through cytopathic effects [50]. Herein, proteolysis of gp120 in HIV-1-infected patients was proposed to generate GAPs that might form protease-resistant amyloid fibrils [51] and, as a result, promote HIV-1 infection.

Neither GAPs nor the GEVIs were found in the blood. However, they were found in tissues. LNs are the main reservoir for HIV, where abundant target cells reside for persistent viral infection and where the drug concentration is much lower than that in blood. Under these conditions, it should be noted that viral proteins are actively expressed even during latency [52–55]. Therefore, with limited extracellular space, higher cell density and slower dilution kinetics, massive amounts of gp120 might be produced at a concentration several logs higher in the lymphatic microenvironment than in the blood, and it might undergo proteolysis to generate GAPs and GEVIs [56]. T-tau and A $\beta$ 42 are well-known brain biomarkers, and it has been reported that the concentration of these biomarkers in CSF might be 200 times greater than that in blood [57]. In particular, GEVIs show a pronounced ability to increase HIV-1 infectivity when the level of infectious virus is low, resembling the conditions of persistent viral infection in LNs. Moreover, considering that multiple GAPs are expressed in vivo, GEVIs can reach the concentration needed to promote viral infection in vivo, as observed in whole lymphatic fluid from an AIDS patient.

The brain is also a haven for HIV persistence. After infecting the peripheral immune system, HIV-1 can cross the blood-brain barrier (BBB) and invade the CNS. In the pre-ART era, HIV encephalitis was associated with a high viral load in the CSF [58, 59]. Paired CSF HIV RNA is thought to be a proxy for the independent replication of HIV in the brain parenchyma. More than 40% of AIDS patients suffer from cognitive impairments, even in the post-ART era [60]. Our results imply that GAPs/GEVIs in the brain may contribute to neuropathy in patients with HIV/AIDS. Moreover, CSF is one of the main sources of protein biomarkers for identifying neurological diseases. The presence of GAPs/GEVIs observed in the present study might serve as a starting point for the study of CSF diagnostic agents. Acute or subacute neurological manifestations may be heralded by GEVIs/GAPs in the CSF, even in the face of continued blood virological control. The presence of GEVIs, which can increase viral infection, might contribute to residual HIV-1 infection, persistence, and viral rebound in the reservoir. Although the paucity of clinical specimens and ethical considerations should be taken into account, the present study suggests a novel disease biomarker, pathogenic factor, and drug target for AIDS in tissues. The investigation of GAPs/GEVIs in other tissues, such as the gut, vaginal tract, gonads, interstitial fluids, and genital secretions, is highly warranted.

Owing to their attractive features, including high structural stability, nanoscale dimensions, and high stability at elevated temperatures, amyloid-based functional nanomaterials have become ideal candidates for the design of intriguing applications in biomedicine and nanotechnology, such as tissue engineering, drug delivery, adhesive materials, biodegradable nanocomposites, and biosensors [61–63]. All GAPs are derived from  $\beta$ -strand fragments in gp120. These  $\beta$ -strand peptides most likely maintain strand structures that favor self-stacking, leading to the easy formation of amyloid fibrils in vitro. The results of the present work are similar to those of Nyström [64]. That is, the amyloidogenic motif sequences in a protein might serve as precursors for designing functional amyloid fibrils.

One of the best-known pathogenic characteristics of amyloids is their cytotoxicity to target cells, which is associated with approximately 50 amyloid diseases in humans. For example, A $\beta$ ,  $\alpha$ -synuclein, and Tau are toxic to neuronal cells in Alzheimer's disease (AD), Parkinson's disease (PD) and prion disease, respectively [65]. Amylin is toxic to  $\beta$ -cells in type II diabetes [66], and immunoglobulin light chain fibrils are toxic to cardiomyocytes in light chain amyloidosis [67]. Despite differences in etiology, primary sequences, and morphologies, the aggregation of mature fibrils and soluble oligomers may cause cellular toxicity by inducing membrane damage, endoplasmic reticulum stress, autophagy disruption, mitochondrial dysfunction, inflammation, or apoptosis [66, 68]. In addition to promoting an increase in viral infection, GAPs or GEVIs might induce toxicity to neurons and lymphocytes, which could, in turn, result in HIV-1-associated neurological complications and the loss of immune cells, respectively. Although amyloid fibrils were found in one out of four brains from HIV patients in the present work, the level of GEVIs might be related to the severity of HIV-1-associated neurological impairment, which deserves further investigation.

The presence of amyloid fibril-forming  $\beta$ -strand peptides is implicated in decreasing the antiviral efficacy of clinically available ARVs. Currently, one of the major obstacles in HIV/AIDS therapeutics is the emergence of drug resistance [69]. Viral mutations are the commonly accepted cause of drug resistance [70]. However, the reduction in the effectiveness of an ARV in the presence of amyloid fibrils formed by degraded viral proteins may be an innovative version of so-called "drug resistance" in vivo. Treatment of this disease is made more difficult by insufficient drug penetration into lymph tissues [71], which is where maximal GEVI activity occurs.

Host proteins undergo proteolysis and generate functional peptides/fibrils, such as amyloidogenic peptides found in amyloidosis, seminal amyloid fibrils that enhance the sexual transmission of viruses [14], and host defense antiviral peptides [72–74]. The results herein suggest the significant role of other type I transmembrane glycoproteins that might also facilitate viral infection by forming amyloid fibrils via proteolysis. Ongoing studies have confirmed that some viral glycoproteins hijack a mechanism of action similar to that of gp120 to form amyloid fibrils that, in turn, similarly promote viral infection (unpublished data) to varying degrees, depending on the amyloid fibrils in question. Additionally, several viruses might not be sensitive to the promotion of viral infection by amyloid fibrils (unpublished data). The proteolysis of viral glycoproteins in vivo is a complex process involving host-viral clearance and persistence, viral lethality, and the complicated tissue microenvironment for protein folding, including factors such as pH, isoelectric point, ionic strength, temperature, protein concentration and the secondary structure of proteins [75]. However, whether the formation of amyloid fibrils that increase viral infectivity is a common feature of viral glycoproteins has yet to be elucidated.

These findings broaden our understanding of gp120 as a contributing factor to the increase in pathogenesis of HIV-1 caused by the production of GAPs and GEVIs, as well as suggesting corresponding therapeutic strategies.

## MATERIALS AND METHODS

### Cell culture

MT-2 and TZM-bl cells were obtained from the NIH HIV Reagent Program. CEMx 174 5.25 M7 cells were kindly provided by C. Cheng-Mayer of the Aaron Diamond AIDS Research Center. HEK-293T cells were kindly provided by Prof. Lu of Fudan University. The following primary antibodies were used: rabbit gp120 antibody (11233-RP02, Sino Biological; PA1-73097, Thermo Fisher), anti-rabbit IgG, HRP-linked antibody (7074 V, Cell Signaling), normal rabbit IgG (2729, Cell Signaling), goat anti-rabbit IgG (FITC) (ab6717, Abcam), goat anti-rabbit IgG labeled with Alexa Fluor® 647 (ab150083, Abcam), and colloidal gold-conjugated goat anti-rabbit IgG (BS-0295G, Bioss Antibodies Co.).

HIV-1 strains were obtained from the NIH HIV Reagent Program. HIV-1 SF162, NL4-3, and the HIV-1 81A and NL4-3 infectious molecular clones were kindly provided by Jan Münch of Ulm University. Clone viruses were produced as previously described [17].

Peptide arrays, the HIV-1 subtype B (MN) Env region, and antiviral agents were obtained from the NIH HIV Reagent Program. Recombinant gp120<sub>JRFL</sub> was purchased from Haiyuan Biotechnology. Thioflavin T and Congo red were purchased from Sigma–Aldrich. Plasmin and thrombin B were purchased from Shanghai Yuanye Bio-Technology Co., and fucosidase was purchased from ProSpec. The luciferase assay system was obtained from Promega. A PROTEOSTAT® Aggresome detection kit was purchased from Enzo Life Sciences.

### Ethics statement

Regarding the lymph node tissues of AIDS patients, human subjects were enrolled in this study with written informed consent approved by The Third People's Hospital of Kunming. CSF samples were isolated from four HIV-1/AIDS patients and two healthy volunteers from Beijing You' An Hospital, and written informed consent was obtained from the study participants and/or their legal guardians. All the experiments were performed in accordance with the approved guidelines and regulations.

### Synthesis of peptides

All chemically synthesized peptides (>95% purity) used in this study were synthesized by Scilight-Peptide (Beijing, China). Peptides were dissolved at a concentration of 5 mM in PBS or DMSO and stored at -20 °C. Fibril formation was initiated by agitation at 37 °C for different durations at 1400 rpm with an Eppendorf Thermomixer.

### Monitoring the formation of amyloid fibrils

Amyloid fibrils were detected by several traditional methods, including ThT staining, Congo red staining, TEM, and CD spectroscopic analysis. For the ThT fluorescence assay, serially diluted peptide solutions (10 µL) were mixed with 190 µL of ThT working solution at 50 µM. Fluorescence was measured following 5 min of incubation at  $\lambda_{\text{ex}} = 452$  nm and  $\lambda_{\text{em}} = 485$  nm using a fluorescence plate reader (Infinite M1000, Tecan) [24]. For the Congo red staining assay, 10 µL of peptide solution at various concentrations was incubated with 90 µL of Congo red solution (Sigma) at room temperature for 30 min and then centrifuged for 15 min at 13,000 rpm. The pellets were dissolved in 50 µL of DMSO, and the signal density was determined at an OD 490–650 nm using an ELISA reader (Infinite M1000, Tecan). CD was applied to detect the typical  $\beta$ -sheet structure of amyloid fibrils. CD spectra were collected from 190 to 280 nm with a scan speed of 50 nm min<sup>-1</sup>, bandwidth of 1 nm and time constant of 2 s on a J-715 spectrometer (Jasco, Japan) at 20 °C. A blank spectrum was subtracted from each spectrum. The shape of the amyloid fibrils was visualized via TEM as previously described [76]. The peptide suspension (50 µM) was adsorbed onto glow-discharged carbon-coated grids for 2 min. The grids were then stained with 2% phosphotungstic acid for 2 min. Fibrils were detected via an H-7650 TEM (Hitachi Limited, Tokyo, Japan). For enzymatic degradation experiments, the mixtures were absorbed onto grids, and the fibrillary shape was analyzed as described above. For the detection of viral infection, the lymphatic leakage and CSF were inactivated with a 2% volume of glutaraldehyde solution at room temperature for 20 min before the samples were loaded onto the grids as described above.

### Viral production

CCR5-tropic HIV-1 SF162, CXCR4-tropic HIV-1 NL4-3, and dual-tropic HIV-1 81A and NL4-3 were produced as previously described [17]. In brief, plasmids encoding proviral DNA were transfected by PEI into HEK-293T cells. Supernatants containing virions were collected 48 h post-transfection

and then centrifuged at 800 rpm for 10 min to remove cell debris. The concentrations of the viruses in the supernatants were determined via ELISA for the p24 antigen [77], and the proteins were stored at -80 °C until use.

The laboratory-adapted strain HIV-1 IIB and primary HIV-1 strains were propagated in MT-2 cells or PBMCs. Briefly, cells were infected with viruses, and after a 4-day or 7-day incubation, cell-free supernatants were collected and then stored at -80 °C.

### HIV-1 infectivity assays

To observe the enhancing effect of amyloid fibrils on HIV-1 infectivity in TZM-bl cells, amyloids or lymphatic leakage products at the indicated concentrations were pretreated with HIV-1 (2 ng of p24) for 5 min at room temperature. The mixtures were added to TZM-bl cells. To minimize the toxic effects mediated by the prolonged exposure of the target cells to amyloids or by lymphatic leakage, the medium was replaced after 3 h, and infection was assayed two days later by determining the luciferase activities.

HIV-1 infectivity in MT-2 or CEMx M7 cells was performed as described above, except that infection was determined by quantifying p24 values 3 days post-infection as described elsewhere [78].

### Virus pull-down assay

The binding of HIV-1 SF162 to amyloid fibrils was determined by a virus pull-down assay [17]. Briefly, fibrils at various concentrations were mixed with the virus (100 ng/mL p24) for 30 min at 37 °C, followed by centrifugation at 5000 rpm for 5 min to pellet the fibrils and bound virions. The infectivity of HIV-1 bound to the pellet was evaluated by ELISA.

### Confocal microscopy detection of HIV-1 binding to amyloid fibrils and cells

The eGFP-labeled virions (R5-tropic) were prepared as described previously [79]. Amyloid fibrils were stained with Proteostat dye as recommended by the manufacturer and incubated 1:1 with eGFP-labeled HIV-1 virions (10 ng p24) at 37 °C for 20 min. Samples were then centrifuged at 5000 rpm for 3 min and imaged using a laser-scanning Nikon A1 confocal microscope (Nikon, Japan). Proteostat and eGFP were excited by using 561 nm and 488 nm laser lines, respectively, and the emissions were collected using appropriate beam splitters.

To visualize the colocalization of amyloid fibrils, viruses, and target cells, the eGFP-HIV-1-amyloid complex, described above, was incubated with TZM-bl cells stained with a cytoplasmic dye as described above. Then, the cells were imaged by confocal microscopy.

### Enzymatic degradation of gp120<sub>JRFL</sub> in vitro

HIV-1 gp120<sub>JRFL</sub> (20 µg) was digested with the indicated enzymes at 37 °C in 200 µL of buffer. Aliquots (5 µL) were taken at the indicated time points, and the degradation of gp120 was evaluated via SDS-PAGE with Coomassie blue. At the 72 h time point, the reaction was stopped by heating in a water bath at 56 °C for 30 min. Then, 10 µL of the digested sample was adsorbed onto the grid for TEM analysis as described above, and the remaining sample was subjected to ultrafiltration (with a 3 kDa cutoff) to collect peptide fragments, which were subsequently lyophilized and stored at -80 °C until LC-MS/MS analysis.

### Collection of HIV-1 infection samples

MT-2 cells and CEMx M7 cells were infected with HIV-1 IIB and HIV-1 SF162, respectively, at 100 TCID<sub>50</sub> (50% tissue culture infective dose) overnight. The culture supernatants were subsequently changed to fresh medium. To minimize the effects of serum on subsequent LC-MS/MS analysis, the culture medium was supplemented with only 2% FBS. On the fourth day post-infection, half of the supernatants were replaced with fresh medium. On the seventh day post-infection, the supernatants were collected by centrifugation at 800 rpm to remove the cells. A portion of the supernatant was heated at 56 °C for 30 min to inactivate the virus before being stored at -80 °C for immunofluorescence analysis and TEM analysis, as described below. The remaining supernatants were treated with mild acid (acetic acid, pH 3.3) to disrupt potential peptide/peptide or peptide/protein interactions. Then, the mixtures were immediately subjected to ultrafiltration (3-kDa cutoff) for the enrichment of peptides with low molecular weights. The filtrate fractions were lyophilized and stored at -80 °C for further LC-MS/MS analysis.

### Lymphatic leakage assay

Lymphatic leakage was collected from an AIDS patient who underwent LN dissection before cervical cancer surgery. The samples were supplemented with a cocktail of protease inhibitors. Lymphatic leakage was centrifuged at 1000 rpm for 15 min at 4 °C. Then, the supernatants were heated at 56 °C for 30 min for immunofluorescence and LC–MS/MS analysis. For TEM analysis, the supernatants were inactivated with 2% glutaraldehyde for 20 min, then packaged and stored at –80 °C. Inactivated samples were confirmed by determining infection in TZM-bl cells.

For LC–MS/MS preparation, RIPA lysis and extraction buffer were used to extract and homogenize the peptides from the remaining supernatants. The mixture was subsequently centrifuged at 12,000 rpm for 10 min, after which the supernatant was collected. Peptides less than 3 kDa in length were then collected and quantified with the Pierce™ BCA Protein Assay Kit. Before LC–MS/MS analysis, the peptides were reduced by 10 mM DTT at 56 °C for 1 h and alkylated by 50 mM iodoacetamide at room temperature in the dark for 40 min. Salt was removed from the samples using a laboratory-made C18 tip. The extracted peptides were lyophilized to near dryness.

### LC–MS/MS analysis

The samples were analyzed using an Eksigent NanoLC-Ultra system coupled to an AB Sciex Triple TOF 5600-plus mass spectrometer. Five microliters of each sample was chromatographically separated using a gradient from 2% mobile phase A (0.1% formic acid, 2% acetonitrile) to 35% mobile phase B (0.1% formic acid, 90% acetonitrile) after direct injection onto a 15-cm PicoFrit emitter (New Objective) packed to 15 cm with Magic C18 AQ 3- $\mu$ m 200-Å stationary phase. Mass spectra were recorded in the range of 350–1500 m/z for 250 ms. In tandem mass spectrometry mode, the thirty most intense peaks with charge states of 2–5 were selected for fragmentation, and MS2 spectra were collected in the range of 50–2000 m/z. Precursor ions were excluded from reselection for 15 s. Each sample was run twice on the mass spectrometer.

### Data analysis

The raw MS/MS data were analyzed using ProteinPilot software version 4.5 (AB Sciex) for peptide matching and identification. The Paragon algorithm, which was integrated into ProteinPilot, was employed against the UniProt *Bos taurus* database. To optimize the number of identified proteins, a filter with strict cutoff criteria was applied, including an unused ProScore <1.3 and a minimum of one distinct peptide identified. The parameters were set as follows: Triple TOF 5600 instrument, identified sample type, biological modifications selected as the ID focus, and thorough search. An automatic decoy database search strategy was employed to estimate the false discovery rate (FDR) using Proteomics System Performance Evaluation Pipeline (PSPEP) software, which is integrated into ProteinPilot software. Only proteins with at least one unique peptide and an unused value greater than 1.3 were considered for further analysis. The targeted peptides were identified through a database search of HIV sequences.

### Detection of gp120-derived amyloid peptides by double staining with an anti-gp120 polyclonal antibody and Proteostat

HIV-1 infectivity samples or lymphatic leakage from an AIDS patient were incubated with rabbit anti-gp120 polyclonal antibody or normal rabbit IgG overnight at 4 °C. The samples were fixed with 4% paraformaldehyde at room temperature for 15 min, followed by three washes with PBS. The samples were then blocked with 10% goat serum and treated with an FITC-conjugated secondary antibody for 1 h in the dark. After washing three times with PBS, the samples were counterstained with Proteostat as recommended by the manufacturer. The samples were subsequently imaged using a laser-scanning Nikon A1 confocal microscope (Nikon, Japan). Proteostat and FITC were excited using 561 nm and 488 nm laser lines, respectively, and the emissions were collected using appropriate beam splitters.

### Immunogold labeling for TEM

Five microliter droplets of HIV-1 infection samples or lymphatic leakage fluid were placed on a Formvar-coated copper grid and incubated for 5 min. The grid was washed three times (10 s each) with 50  $\mu$ L droplets of PBS, pH 7.4. Excess solvent was carefully soaked off with filter paper, and then a 50  $\mu$ L droplet of 5% bovine serum albumin in PBS was added for 15 min. Afterward, the grid was washed with a 50  $\mu$ L droplet of buffer. Excess solvent was

removed with filter paper, and the grid was incubated for 1 h with 50  $\mu$ L of either rabbit anti-gp120 polyclonal antibody or normal rabbit IgG, covered with a Petri dish. The grid was washed in PBS as described above before a 50  $\mu$ L droplet of goat anti-rabbit antibody conjugated to 10 nm gold particles was applied. The grid was then washed again with a 50  $\mu$ L droplet of PBS containing 0.05% Tween 20 for 20 s and three droplets of 50  $\mu$ L of water for 10 s each. Finally, the grid was stained using a series of three 50  $\mu$ L droplets containing 2% phosphotungstic acid (2 min each) and then dried with filter paper. All steps were carried out at room temperature. Samples labeled with an anti-gp120 antibody and the corresponding control rabbit IgG were visualized with an H-7650 TEM (Hitachi Limited, Tokyo, Japan) operated at an acceleration voltage of 80 kV [25].

### Copolymerization of fluorescently labeled GAPs

A stock solution of each GAP in DMSO at a final molar ratio of 1:1 or 1:1:1 was mixed gently. The mixed samples were diluted in PBS to a suitable concentration for the detection of amyloid fibril formation and determination of the enhancement of viral infection as described above.

### Human tissue specimens and immunochemical staining

Congo red staining and immunohistochemistry in situ double staining were combined to detect naturally occurring gp120-derived amyloid fibrils in 4  $\mu$ m thick paraffin-embedded axillary LNs from AIDS patients. Sections were deparaffinized in xylene and then rehydrated in graded ethanol. Then, 3% hydrogen peroxide/methanol was used to block endogenous peroxidase activity. For antigen retrieval, the sections were boiled in 0.01 M citrate buffer (pH 6.0) for 30 min and washed with PBS (pH 7.4). The sections were blocked with 10% goat serum at room temperature for 30 min. The slides were incubated with primary rabbit anti-gp120 at 4 °C overnight. HRP-conjugated anti-rabbit IgG and DAB were used to visualize the positive sites. Sections were then stained with 0.2% Congo red (Sigma–Aldrich) in alkaline solution, and hematoxylin was used for counterstaining. After being sealed with neutral tree gum, sections were prepared for visualization by a Nikon ECLIPSE 90i microscope. Immunofluorescence staining was also used to detect amyloid deposition in paraffin-embedded axillary LNs from AIDS patients. Briefly, sections were incubated with antibodies against gp120 overnight at 4 °C. After washing with PBS, the samples were treated with an anti-rabbit secondary antibody labeled with FITC and then incubated with Proteostat at room temperature for 30 min. The nuclei were stained with Hoechst. Fluorescence images were acquired using an Axio Observer microscope (Zeiss).

### Collection of CSF samples from HIV-1-infected patients and healthy persons

CSF was collected (5 mL/patient) by lumbar puncture. Vital signs and symptoms of intracranial hypertension were examined before CSF collection. Pressure was measured after puncture. The patient remained supine without a pillow for 2–4 h, after which vital signs were closely observed. CSF test indicators included CSF parameters (glucose, chloride, urine cerebrospinal fluid protein, and mononuclear cells) and CSF biochemical parameters (white blood cells and cerebrospinal fluid viral load).

### Identification of amyloidogenic peptides in CSF by LC–MS/MS

In brief, CSF samples (600  $\mu$ L) were centrifuged at 2200 rpm for 10 min to remove cellular debris. RIPA lysis and extraction buffer were used to extract and homogenize the peptides from the CSF supernatants. Peptides less than 10 kDa in length were collected and quantified with the Pierce™ BCA Protein Assay Kit. Next, 20  $\mu$ g of peptide sample was reduced by 10 mM DTT at 37 °C for 1 h and alkylated by 50 mM iodoacetamide at room temperature in the dark for 40 min. The resulting peptide samples were lyophilized to near dryness and resuspended in 2–20  $\mu$ L of 0.1% formic acid/2% acetonitrile before LC–MS/MS analysis.

The samples were subjected to an Orbitrap Eclipse mass spectrometer (Thermo Fisher Scientific, USA). The spray voltage was 2.2 kV. The capillary temperature was 270 °C. The MS parameters used were as follows: resolution: 70000 at 400 m/z; MS precursor m/z range: 350.0–1500.0; MS/MS parameters: activation type; HCD; normalized coll; energy: 28.0; activation time: 120.000; and data-dependent MS/MS: up to the top 20 most intense peptide ions from the preview scan in the Orbitrap.

The raw MS files were analyzed and searched against the peptide database using MaxQuant (1.6.2.10). The parameters were set as follows: protein modifications were carbamidomethylation (C) (fixed); oxidation (M)

(variable); the enzyme specificity was set to unspecific; the precursor ion mass tolerance was set to 20 ppm; and the MS/MS tolerance was set to 20 ppm. Only peptides identified with high confidence were chosen for downstream protein identification analysis.

## REFERENCES

- Pu J, Wang Q, Xu W, Lu L, Jiang S. Development of protein- and peptide-based HIV entry inhibitors targeting gp120 or gp41. *Viruses*. 2019;11:705.
- Ronaldson PT, Bendayan R. HIV-1 viral envelope glycoprotein gp120 triggers an inflammatory response in cultured rat astrocytes and regulates the functional expression of P-glycoprotein. *Mol Pharm*. 2006;70:1087–98.
- Cossarizza A. Apoptosis and HIV infection: about molecules and genes. *Curr Pharm Des*. 2008;14:237–44.
- He X, Yang W, Zeng Z, Wei Y, Gao J, Zhang B, et al. NLRP3-dependent pyroptosis is required for HIV-1 gp120-induced neuropathology. *Cell Mol Immunol*. 2020;17:283–99.
- Smith LK, Kuhn TB, Chen J, Bamburg JR. HIV associated neurodegenerative disorders: a new perspective on the role of lipid rafts in Gp120-mediated neurotoxicity. *Curr HIV Res*. 2018;16:258–69.
- Anand AR, Rachel G, Parthasarathy D. HIV proteins and endothelial dysfunction: implications in cardiovascular disease. *Front Cardiovasc Med*. 2018;5:185.
- Qian Y, Che X, Jiang J, Wang Z. Mechanisms of blood-retinal barrier disruption by HIV-1. *Curr HIV Res*. 2019;17:26–32.
- Cotter EJ, Malizia AP, Chew N, Powderly WG, Doran PP. HIV proteins regulate bone marker secretion and transcription factor activity in cultured human osteoblasts with consequent potential implications for osteoblast function and development. *AIDS Res Hum Retroviruses*. 2007;23:1521–30.
- Sipe JD, Cohen AS. Review: history of the amyloid fibril. *J Struct Biol*. 2000;130:88–98.
- Jaunmuktane Z, Mead S, Ellis M, Wadsworth JD, Nicoll AJ, Kenny J, et al. Evidence for human transmission of amyloid-beta pathology and cerebral amyloid angiopathy. *Nature*. 2015;525:247–50.
- Marin-Moreno A, Fernández-Borges N, Espinosa JC, Andréoletti O, Torres JM. Transmission and replication of prions. *Prog Mol Biol Transl Sci*. 2017;150:181–201.
- Epstein EA, Chapman MR. Polymerizing the fibre between bacteria and host cells: the biogenesis of functional amyloid fibres. *Cell Microbiol*. 2008;10:1413–20.
- Gebbink MF, Claessen D, Bouma B, Dijkhuizen L, Wösten HA. Amyloids—a functional coat for microorganisms. *Nat Rev Microbiol*. 2005;3:333–41.
- Münch J, Rücker E, Ständker L, Adermann K, Goffinet C, Schindler M, et al. Semen-derived amyloid fibrils drastically enhance HIV infection. *Cell*. 2007;131:1059–71.
- Roan NR, Müller JA, Liu H, Chu S, Arnold F, Stürzel CM, et al. Peptides released by physiological cleavage of semen coagulum proteins form amyloids that enhance HIV infection. *Cell Host Microbe*. 2011;10:541–50.
- Röcker A, Roan NR, Yadav JK, Fändrich M, Münch J. Structure, function and antagonism of semen amyloids. *Chem Commun*. 2018;54:7557–69.
- Tan S, Li L, Lu L, Pan C, Lu H, Oksov Y, et al. Peptides derived from HIV-1 gp120 co-receptor binding domain form amyloid fibrils and enhance HIV-1 infection. *FEBS Lett*. 2014;588:1515–22.
- Jeyashekar NS, Sadana A, Vo-Dinh T. Protein amyloidose misfolding: mechanisms, detection, and pathological implications. *Methods Mol Biol*. 2005;300:417–35.
- Kwong PD, Wyatt R, Robinson J, Sweet RW, Sodroski J, Hendrickson WA. Structure of an HIV gp120 envelope glycoprotein in complex with the CD4 receptor and a neutralizing human antibody. *Nature*. 1998;393:648–59.
- Pancera M, Majeed S, Ban YE, Chen L, Huang CC, Kong L, et al. Structure of HIV-1 gp120 with gp41-interactive region reveals layered envelope architecture and basis of conformational mobility. *Proc Natl Acad Sci USA*. 2010;107:1166–71.
- Singh AK, Jiang Y, Gupta S. Effects of chronic alcohol drinking on receptor-binding, internalization, and degradation of human immunodeficiency virus 1 envelope protein gp120 in hepatocytes. *Alcohol*. 2007;41:591–606.
- Chen J, Ren R, Yu F, Wang C, Zhang X, Li W, et al. A degraded fragment of HIV-1 Gp120 in rat hepatocytes forms fibrils and enhances HIV-1 infection. *Biophys J*. 2017;113:1425–39.
- Kwong PD, Wyatt R, Majeed S, Robinson J, Sweet RW, Sodroski J, et al. Structures of HIV-1 gp120 envelope glycoproteins from laboratory-adapted and primary isolates. *Structure*. 2000;8:1329–39.
- Nilsson MR. Techniques to study amyloid fibril formation in vitro. *Methods*. 2004;34:151–60.
- Usmani SM, Zirafi O, Müller JA, Sandi-Monroy NL, Yadav JK, Meier C, et al. Direct visualization of HIV-enhancing endogenous amyloid fibrils in human semen. *Nat Commun*. 2014;5:3508.
- Gosai A, Hau Yeah BS, Nilsen-Hamilton M, Shrotriya P. Label free thrombin detection in presence of high concentration of albumin using an aptamer-functionalized nanoporous membrane. *Biosens Bioelectron*. 2019;126:88–95.
- Shan M, Yang D, Dou H, Zhang L. Fucosylation in cancer biology and its clinical applications. *Prog Mol Biol Transl Sci*. 2019;162:93–119.
- Roan NR, Münch J, Arhel N, Mothes W, Neidleman J, Kobayashi A, et al. The cationic properties of SEVI underlie its ability to enhance human immunodeficiency virus infection. *J Virol*. 2009;83:73–80.
- Yolamanova M, Meier C, Shaytan AK, Vas V, Bertoncini CW, Arnold F, et al. Peptide nanofibrils boost retroviral gene transfer and provide a rapid means for concentrating viruses. *Nat Nanotechnol*. 2013;8:130–6.
- Neurath AR, Strick N, Li YY. Role of seminal plasma in the anti-HIV-1 activity of candidate microbicides. *BMC Infect Dis*. 2006;6:150.
- Zirafi O, Kim KA, Roan NR, Kluge SF, Müller JA, Jiang S, et al. Semen enhances HIV infectivity and impairs the antiviral efficacy of microbicides. *Sci Transl Med*. 2014;6:262ra157.
- Young LM, Tu LH, Raleigh DP, Ashcroft AE, Radford SE. Understanding copolymerization in amyloid formation by direct observation of mixed oligomers. *Chem Sci*. 2017;8:5030–40.
- Chen J, Ren R, Tan S, Zhang W, Zhang X, Yu F et al. A peptide derived from the HIV-1 gp120 coreceptor-binding region promotes formation of PAP248-286 amyloid fibrils to enhance HIV-1 infection. *PLoS One*. 2015;10:e0144522.
- Linke RP, Gärtner HV, Michels H. High-sensitivity diagnosis of AA amyloidosis using Congo red and immunohistochemistry detects missed amyloid deposits. *J Histochem Cytochem*. 1995;43:863–9.
- Menter T, Bachmann M, Grieshaber S, Tzankov A. A more accurate approach to amyloid detection and subtyping: combining in situ Congo red staining and immunohistochemistry. *Pathobiology*. 2017;84:49–55.
- Buzy J, Breneman DE, Pert CB, Martin A, Salazar A, Ruff MR. Potent gp120-like neurotoxic activity in the cerebrospinal fluid of HIV-infected individuals is blocked by peptide T. *Brain Res*. 1992;598:10–18.
- Kajava AV, Baxa U, Steven AC. Beta arcades: recurring motifs in naturally occurring and disease-related amyloid fibrils. *FASEB J*. 2010;24:1311–9.
- Parren PW, Burton DR, Sattentau QJ. HIV-1 antibody-debris or virion? *Nat Med*. 1997;3:366–7.
- Moore JP, McKeating JA, Weiss RA, Sattentau QJ. Dissociation of gp120 from HIV-1 virions induced by soluble CD4. *Science*. 1990;250:1139–42.
- Hart TK, Kirsh R, Ellens H, Sweet RW, Lambert DM, Petteway SR Jr et al. Binding of soluble CD4 proteins to human immunodeficiency virus type 1 and infected cells induces release of envelope glycoprotein gp120. *Proc Natl Acad Sci USA*. 1991;88:2189–93.
- Perelson AS, Neumann AU, Markowitz M, Leonard JM, Ho DD. HIV-1 dynamics in vivo: virion clearance rate, infected cell life-span, and viral generation time. *Science*. 1996;271:1582–6.
- Ho DD, Neumann AU, Perelson AS, Chen W, Leonard JM, Markowitz M. Rapid turnover of plasma virions and CD4 lymphocytes in HIV-1 infection. *Nature*. 1995;373:123–6.
- Cummins NW, Rizza SA, Badley AD. How much gp120 is there? *J Infect Dis*. 2010;201:1273–4.
- Reeds DN, Cade WT, Patterson BW, Powderly WG, Klein S, Yarasheski KE. Whole-body proteolysis rate is elevated in HIV-associated insulin resistance. *Diabetes*. 2006;55:2849–55.
- Ponomarenko NA, Durova OM, Vorobiev II, Aleksandrova ES, Telegin GB, Chamborant OG, et al. Catalytic antibodies in clinical and experimental pathology: human and mouse models. *J Immunol Methods*. 2002;269:197–211.
- Wolf DA, Dholakia SR, Keherly MJ, Rodriguez-Wolf MG, Cloyd MW, Gelman BB. Proteolysis in the myelopathy of acquired immunodeficiency syndrome: preferential loss of the C-8 component of myelin basic protein. *Lab Invest*. 1997;77:513–23.
- Paul S, Karle S, Planque S, Taguchi H, Salas M, Nishiyama Y et al. Naturally occurring proteolytic antibodies: selective immunoglobulin M-catalyzed hydrolysis of HIV gp120. *J Biol Chem*. 2004;279:39611–9.
- Ponomarenko NA, Vorobiev II, Alexandrova ES, Reshetnyak AV, Telegin GB, Khaidukov SV, et al. Induction of a protein-targeted catalytic response in autoimmune prone mice: antibody-mediated cleavage of HIV-1 glycoprotein GP120. *Biochemistry*. 2006;45:324–30.
- Planque S, Nishiyama Y, Taguchi H, Salas M, Hanson C, Paul S. Catalytic antibodies to HIV: physiological role and potential clinical utility. *Autoimmun Rev*. 2008;7:473–9.
- Willey RL, Bonifacino JS, Potts BJ, Martin MA, Klausner RD. Biosynthesis, cleavage, and degradation of the human immunodeficiency virus 1 envelope glycoprotein gp160. *Proc Natl Acad Sci USA*. 1988;85:9580–4.
- Fowler DM, Koulouf AV, Balch WE, Kelly JW. Functional amyloid from bacteria to humans. *Trends Biochem Sci*. 2007;32:217–24.
- Fletcher CV, Staskus K, Wietgreffe SW, Rothenberger M, Reilly C, Chipman JG, et al. Persistent HIV-1 replication is associated with lower antiretroviral drug concentrations in lymphatic tissues. *Proc Natl Acad Sci USA*. 2014;111:2307–12.

53. Anderson EM, Maldarelli F. The role of integration and clonal expansion in HIV infection: live long and prosper. *Retrovirology*. 2018;15:71.
54. Imamichi H, Smith M, Adelsberger JW, Izumi T, Scrimieri F, Sherman BT, et al. Defective HIV-1 proviruses produce viral proteins. *Proc Natl Acad Sci USA*. 2020;117:3704–10.
55. Yukl SA, Shergill AK, Ho T, Killian M, Girling V, Epling L, et al. The distribution of HIV DNA and RNA in cell subsets differs in gut and blood of HIV-positive patients on ART: implications for viral persistence. *J Infect Dis*. 2013;208:1212–20.
56. Klasse PJ, Moore JP. Is there enough gp120 in the body fluids of HIV-1-infected individuals to have biologically significant effects? *Virology*. 2004;323:1–8.
57. Shahim P, Zetterberg H, Simrén J, Ashton NJ, Norato G, Schöhl M et al. Association of plasma biomarker levels with their CSF concentration and the number and severity of concussions in professional athletes. *Neurology*. 2022;99:E347–E354.
58. Canestri A, Lescuré FX, Jaureguierry S, Moulignier A, Amiel C, Marcelin AG et al. Discordance between cerebral spinal fluid and plasma HIV replication in patients with neurological symptoms who are receiving suppressive antiretroviral therapy. *Clin Infect Dis*. 2010;50:773–8.
59. Edén A, Fuchs D, Hagberg L, Nilsson S, Spudich S, Svennerholm B, et al. HIV-1 viral escape in cerebrospinal fluid of subjects on suppressive antiretroviral treatment. *J Infect Dis*. 2010;202:1819–25.
60. Wang Y, Liu M, Lu Q, Farrell M, Lappin JM, Shi J et al. Global prevalence and burden of HIV-associated neurocognitive disorder: A meta-analysis. *Neurology*. 2020;95:e2610–e2621.
61. Díaz-Caballero M, Navarro S, Ventura S. Functionalized prion-inspired amyloids for biosensor applications. *Biomacromolecules*. 2021;22:2822–33.
62. Wang W, Gil-García M, Ventura S. Dual antibody-conjugated amyloid nanorods to promote selective cell-cell interactions. *ACS Appl Mater Interfaces*. 2021;13:14875–84.
63. Knowles TP, Buehler MJ. Nanomechanics of functional and pathological amyloid materials. *Nat Nanotechnol*. 2011;6:469–79.
64. Nyström S, Hammarstrom P. Amyloidogenesis of SARS-CoV-2 Spike Protein. *J Am Chem Soc*. 2022;144:8945–50.
65. Gadad BS, Britton GB, Rao KS. Targeting oligomers in neurodegenerative disorders: lessons from alpha-synuclein, tau, and amyloid-beta peptide. *J Alzheimers Dis*. 2011;24:223–232.
66. Marmontini C, Branco RCS, Boschero AC, Kurauti MA. Islet amyloid toxicity: from genesis to counteracting mechanisms. *J Cell Physiol*. 2022;237:1119–42.
67. Marin-Argany M, Lin Y, Misra P, Williams A, Wall JS, Howell KG et al. Cell damage in light chain amyloidosis: fibril internalization, toxicity and cell-mediated seeding. *J Biol Chem*. 2016;291:19813–25.
68. Lee S, Choi MC, Al Adem K, Lukman S, Kim TY. Aggregation and cellular toxicity of pathogenic or non-pathogenic proteins. *Sci Rep*. 2020;10:5120.
69. Trono D, Van Lint C, Rouzioux C, Verdin E, Barré-Sinoussi F, Chun TW, et al. HIV persistence and the prospect of long-term drug-free remissions for HIV-infected individuals. *Science*. 2010;329:174–80.
70. Calmy A, Pascual F, Ford N. HIV drug resistance. *N. Engl J Med*. 2004;350:2720–1.
71. Popovic M, Tenner-Racz K, Pelsler C, Stellbrink HJ, van Lunzen J, Lewis G et al. Persistence of HIV-1 structural proteins and glycoproteins in lymph nodes of patients under highly active antiretroviral therapy. *Proc Natl Acad Sci USA*. 2005;102:14807–12.
72. Kramer HB, Lavender KJ, Qin L, Stacey AR, Liu MK, di Gleria K, et al. Elevation of intact and proteolytic fragments of acute phase proteins constitutes the earliest systemic antiviral response in HIV-1 infection. *PLoS Pathog*. 2010;6:e1000893.
73. Harms M, Hayn M, Zech F, Kirchhoff F, Münch J. Endogenous peptide inhibitors of HIV entry. *Adv Exp Med Biol*. 2022;1366:65–85.
74. Münch J, Ständker L, Adermann K, Schulz A, Schindler M, Chinnadurai R, et al. Discovery and optimization of a natural HIV-1 entry inhibitor targeting the gp41 fusion peptide. *Cell*. 2007;129:263–75.
75. Wang W, Nema S, Teagarden D. Protein aggregation-pathways and influencing factors. *Int J Pharm*. 2010;390:89–99.
76. Tan S, Li JQ, Cheng H, Li Z, Lan Y, Zhang TT, et al. The anti-parasitic drug suramin potently inhibits formation of seminal amyloid fibrils and their interaction with HIV-1. *J Biol Chem*. 2019;294:13740–54.
77. Tan S, Li W, Li Z, Li Y, Luo J, Yu L, et al. A novel CXCR4 targeting protein SDF-1/54 as an HIV-1 entry inhibitor. *Viruses* 2019;11:874.
78. Li L, He L, Tan S, Guo X, Lu H, Qi Z et al. 3-hydroxyphthalic anhydride-modified chicken ovalbumin exhibits potent and broad anti-HIV-1 activity: a potential microbicide for preventing sexual transmission of HIV-1. *Antimicrob Agents Chemother*. 2010;54:1700–11.
79. Huang JH, Qi Z, Wu F, Kotula L, Jiang S, Chen YH. Interaction of HIV-1 gp41 core with NPF motif in Epsin: implication in endocytosis of HIV. *J Biol Chem*. 2008;283:14994–5002.

## ACKNOWLEDGEMENTS

We thank Yelena Oksov for her help in performing the TEM experiment. This work was supported by grants from the Natural Science Foundation of China (82072276 and 81772194 to ST, 82073898 and 31370781 to SL, and 81630090 to SJ).

## AUTHOR CONTRIBUTIONS

S.T., S.L., and S.J. conceived the study. S.T., W.L., C.Y., S.L., and S.J. contributed to the methodology. S.T., W.L., C.Y., Q.Z., K.L., J.L., Z.L., and F.Y. performed the experiments and analyzed the data. Y.Y.L., Y.X.D., J.L., Y.M.J., J.S.B., L.W., Y.T.Z., T.Z., and J.W. collected the clinical samples. S.T., S.L., and S.J. acquired the funding. S.T., S.L., and S.J. supervised the study. S.T., W.L., and C.Y. drafted the manuscript. S.T., S.L., S.J., L.L., and L.L. reviewed and edited the manuscript.

## COMPETING INTERESTS

The authors declare no competing interests.

## ADDITIONAL INFORMATION

**Supplementary information** The online version contains supplementary material available at <https://doi.org/10.1038/s41423-024-01144-y>.

**Correspondence** and requests for materials should be addressed to Suiyi Tan, Shibo Jiang or Shuwen Liu.

**Reprints and permission information** is available at <http://www.nature.com/reprints>

Springer Nature or its licensor (e.g. a society or other partner) holds exclusive rights to this article under a publishing agreement with the author(s) or other rightsholder(s); author self-archiving of the accepted manuscript version of this article is solely governed by the terms of such publishing agreement and applicable law.